AN ELECTRON MICROPROBE STUDY OF LUMINESCENCE CENTERS IN CASSITERITE

by

Monte R. Hall

Thesis submitted to the Graduate Faculty of the

Virginia Polytechnic Institute

in partial fulfillment for the degree of

MASTER OF SCIENCE

in

Geological Sciences

APPROVED:

Chairman, P. H. Ribbe

G. V. Gibbs

G. C. Grender

F. D. Bloss

R. V. Dietrich

Blacksburg, Virginia

TABLE OF CONTENTS

ACKNOWLEDGMENTS

The writer wishes to express his sincere appreciation to his major advisor, , who initiated this research and supplied the specimens from his original work. has also stimulated the writer's interest in this research through many helpful discussions on the mineralogical significance of cathodoluminescence studies.

Special thanks go to for many stimulating discussions on theoretical crystallography and its relation to solid state physics. Thanks also to

and for reading and constructively criticizing the thesis. The writer also gratefully acknowledges the assistance provided by and

in machining parts for the microprobe modifications.

The Department of Geological Sciences, University of Chicago, the Chicago Natural History Museum, the Smithsonian Institution and

of the University of Hawaii very kindly supplied the cassiterite samples used in this study. of the General Electric Company kindly supplied the calibrated electroluminescent panels which were used as references for spectral calibration of the luminescence measurements. The writer also gratefully acknowledges the assistance o: who typed the thesis and

for drafting many of the figures.

LIST OF TABLES

LIST OF PLATES

LIST OF FIGURES

I. INTRODUCTION

General

Minerals often emit visible luminescence when they are bombarded with energetic electrons -- as during electron-excited x-ray emission microanalysis. Such cathodoluminescence can, when correlated with simultaneous microanalysis, furnish a method for studying chemical zoning and the associated microtexture of minerals. Cathodoluminescence in minerals is usually associated with the presence of impurities and is sensitive to concentrations of a few ppm. The color of luminescence for a particular mineral is often diagnostic of the type of impurity atoms present. Thus, using this effect, the electron microprobe can reveal details of mineral composition and texture which have little effect on optical properties and which are, at best, poorly resolved in x-ray scanning images.

Recent Work

A qualitative survey of potential uses of cathodoluminescence in petrology was made by Smith and Stenstrom (1965) who observed luminescence in quartz, apatite, feldspars, carbonates (including fossils) and some synthetic crystals and glasses. Heinrich (1963) used a photomultiplier tube to detect cathodoluminescence and to produce scanning mode images with the electron microprobe. Kyser and Wittrey (1964) used a grating spectrometer attached to the microprobe optics to study cathodoluminescence due to excess carriers produced

by the electron beam in gallium arsenide. Bahezre, Capitant and Duong (1961) made microscans across a zoned cassiterite for Ti, Fe and Ta impurities, but did not report cathodoluminescence, perhaps because Ta suppresses such luminescence.

Preliminary reports of the cathodoluminescence of cassiterites containing Ti and W as impurity activators were presented as an abstract by title (Ribbe and Hall, 1965) and orally (Hall and Ribbe, 1968). This thesis is an extension of the work reported earlier, involving more detailed microprobe analysis and the development of special instrumental techniques for cathodoluminescence measurements.

II. EXPERIMENTAL PROCEDURE

General

This study was a preliminary one to determine if an electron microprobe could be adapted to make reliable measurements of luminescence intensity and spectral dispersion simultaneously with x-ray measurements of the concentrations of impurity atoms. The observed intensities of cathodoluminescence are typically low; hence a dispersive device of high optical efficiency is required. Interference filters have an effective transmission 10 to 1000 times greater than that for grating or prism monochromators with the same passband and are easily adapted to the light optical system of the microprobe. The filters transmit up to 45% of the light in a passband of 15 to 20 mμ. The spectral resolution obtained with interference filters when making measurements on weak luminophors is as good as that to be obtained with a grating or prism spectrometer for strong luminophors.

Instrumental Modifications

The existing reflecting type optical objective of the microprobe was modified to facilitate the attachment of a dispersive device (narrow band interference filters) and a photomultiplier tube. Modifications consisted of removing the existing window between the microscope illuminator housing and the vacuum chamber, vacuum sealing the illuminator housing and extending it so as to contain a movable plane mirror which deflects the light into the dispersive device (See Fig. 12, Appendix A). Ultraviolet transmitting (Spectrosil) glass was used to pass the light from the modified illuminator housing.

The divergence angle, at the monocular of the microscope, of the luminescence from a finely focussed electron beam is only a few degrees so that interference filters can be placed in the focal plane of the monocular without the necessity of collimation. The photomultiplier was that normally used with the secondary electron detection system. The output of this detector was connected through a micro-ammeter to a recorder for measurements of the luminescence spectrum. An X-Y recorder was used for intensity measurements when line-scanning the sample. In this mode the luminescence or x-ray signal was connected to the "Y" channel while the line scanning sweep voltage was connected to the "X" channel. In this way, consecutive scans were made over the same line on the sample for intensity profiles of luminescence and x-rays. The luminescence scan was always made first in order to minimize losses due to contamination of the specimen surface. The spectral dispersion curves were obtained by inserting calibrated narrow bandpass interference filters between the source and detector. The optical transmission and spectral sensitivity of the combined system of mirrors, windows and photomultiplier detector were approximately determined by making measurements on four standard electroluminescent panels, kindly donated by the General Electric Company. The intensity measurement for each of ten filters covering the range from 400 to 710 mμ were corrected for filter transmission and the above mentioned effects and plotted versus the wavelength calibration for the respective filter.

Measurements in the ultraviolet region (200 to 400 mμ) were corrected only for filter transmission.

Color transparencies were taken on Anscochrome 500 film with a 35 mm. camera attached to the monocular tube. The electron beam was defocussed to cause cathodoluminescence to be emitted from a circular region of about 300 microns in diameter. The electron beam current had to be kept low (~ 0.5 μA) in order to minimize the build-up of a carbonaceous film on the sample surface. The contaminating film selectively absorbs visible luminescence resulting in untrue color exposures. The exposure times required under these conditions were from 5 to 15 minutes.

Specimen Description

Seventeen samples were analyzed in thin section. Two of these, one showing fine yellow-green luminescence zones and one with blue luminescent zones, were remounted on ultraviolet transmitting glass for light absorption measurements. A sample holder was modified to accept a small black lamp (GE type MF2BLB). The transmission of selected regions of the sample was measured and compared with the transmission of the mounting substrate in order to determine the absorption bands corresponding to the luminescence transitions. Another twenty-three samples were mounted in bulk, polished and used for the luminescence photographs and for microanalysis. One of these, from a Malaysian tin mine (specimen MA56417, see Table III, Appendix B), which exhibited

yellow-green luminescence was mounted with a high-temperature cement (Sauereisen) together with a small resistance heater and thermocouple in order to determine the variation of the luminescence emission with sample temperature.

III. SUMMARY OF LUMINESCENCE THEORY

Band-Theory Model

The emission and absorption of radiation by atomic systems is presently understood by the application of quantum mechanics to the case of isolated atoms or ions. The discrete lines of the absorption and emission spectrum for a specific element correspond to allowed transitions between discrete electron energy states which are eigensolutions of the Schrödinger equation for an electron bound by the effective (screened) nuclear potential. The development of the theory for electrons bound by a periodic potential, such as that of a crystal, is due to Bloch (1928), and leads to the energy band model for binding electrons in a crystalline solid. The mutual interaction of ions in a solid causes the discrete states of the isolated atoms to be broadened into nearly continuous bands of allowed electron energy separated by bands of forbidden energy. These bands extend throughout the crystal so that the binding electrons can move freely through the crystal.

An insulator, at low temperatures, is characterized by a wide forbidden energy region separating a normally filled energy band (valence band) from a higher, normally empty band (conduction band). No net electron current can flow in either a completely empty or a completely filled band, and a large concentration of energy is necessary to raise electrons from the filled band into the empty band. In an imperfect insulator, the presence of impurity atoms or other crystal defects locally distorts the periodic crystal field. As a result,

allowable energy states may be interposed in the normally forbidden region; these may be accompanied by the introduction of charge carriers, electrons or holes (electron vacancies). This modified energy band model for imperfect insulators and extrinsic semiconductors (Fig. 1) is applicable to the case of impurity-ion- or crystal-defect-activated luminescence.

Solid-state luminescence may be emitted when electrons in excited states a few ev. above the valence band return to a ground state located near the valence band. A beam of energetic electrons can create a large population of excited states; these may consist of free electrons and holes in the conduction and valence bands, respectively, electrons or holes in quasi-stable levels of the normally forbidden region (traps), or bound electron-hole pairs (excitons) which are electrically neutral and may move through the crystal, transporting excitation energy but no net charge. Cathodoluminescence results when radiative transitions between the energy levels associated with impurity ions are relatively more probable than nonradiative transitions. Such impurity ions (activators) produce "luminescence centers." Such centers can be excited by absorption of excitation energy in the center or by capturing mobile electrons and holes produced elsewhere. Luminescence centers usually provide for momentum conservation in electron-hole recombination. In the absence of luminescence centers electron-hole recombination is more likely to involve indirect transitions which require the creation of phonons of

vibrational energy. Other impurities or defects may introduce additional quenching mechanisms or may provide more effective coupling of excited states to the quenching modes of the 'lattice' vibrations, and are called "killers."

The luminescence process then requires: 1) an efficient means of producing free electron-hole pairs, or excitons; 2) movement of electrons and holes to the vicinity of luminescence centers, and/or high absorption of excitation energy in the center; 3) a high probability of optical transitions occurring in the center compared to the likelihood of energy loss to quenching mechanisms. Hence, the intensity of luminescence will usually increase with the concentration of activator ions and decrease with an increase in the concentration of quenching defects. High temperatures will promote thermal disturbance of the centers and lead to luminescence quenching. An exception to the rule for the variation of intensity with concentration occurs in many systems when the concentration of 'activators' is large enough to cause appreciable long-range distortion of the structure and "concentration quenching" results. When activators are of the substitutional type, luminescence may be enhanced by concentrations up to several weight percent; for interstitial impurities, effective concentrations are much lower.

Figure 1(a) illustrates some basic luminescence processes which may occur. The vertical arrow (labeled 1) indicates the excitation of electrons from the valence band into the conduction band. Horizontal

arrows (2, 2', 2") indicate diffusion of electrons and holes through the crystal to the vicinity of luminescence centers. Vertical arrows (3, 3', 3") indicate recombination of electrons and holes. The first of these (I) indicates return via partially filled energy levels due to an impurity ion which causes local distortion of the crystal field but does not introduce charge defects. Processes II and III represent recombination via acceptor and donor levels respectively. When the direct return from a level of a luminescence center to the ground state is a forbidden transition, the center is an electron or hole trap. Traps are emptied by thermal agitation, resulting in phosphorescence which is characterized by a temperature-dependent long decay time.

Configuration Coordinate Model

The configuration coordinate diagram (Fig. 1(b)) relates absorption and emission processes and the interaction of electronic and vibrational states of the luminescence center. The width of the emission bands, the Stoke's shift of the emission band with respect to the related absorption band, and the temperature dependence of competing radiative versus non-radiative processes can be understood qualitatively by reference to this diagram. The configuration coordinate is a function of the nuclear coordinates of the ions surrounding the center. Total energy in this diagram includes both the electronic and the vibrational energy of the center and has arbitrarily been taken at zero for a thermal equilibrium energy near the top of the valence band. The upper

Figure 1. (a) Composite electron energy band model. Cross-hatched region represents the valence band. Process II after Schön (1942) and Klasens (1946). Process III after Lambe-Klick (1955).

(b) The configuration coordinate diagram for some typical luminescence processes, after von Hippel (1936) and Seitz (1938).

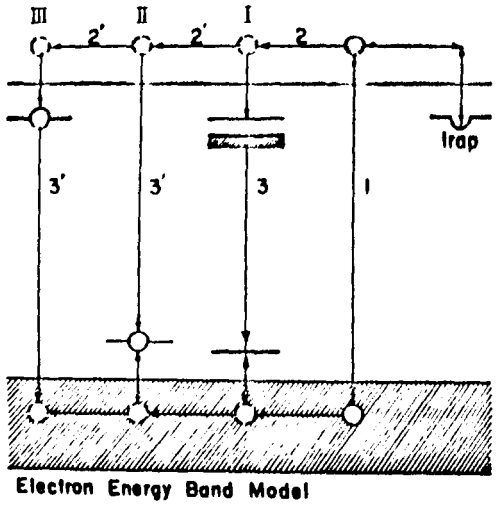

Electron Energy Band Model

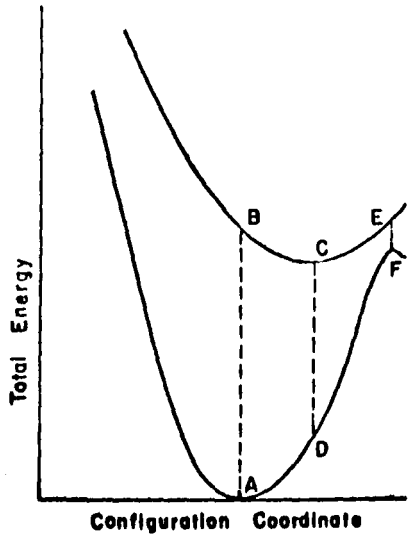

curve represents levels in the conduction band. Transition A-B represents a typical excitation (absorption) process. Motion along the curves (B-C, C-E, or D-A) represents thermal transitions due to vibrational motion near the center. The transition B-C-D-A is a typical radiative return process, while B-E-F-A represents a typical radiationless return to the ground state.

IV. EXPERIMENTAL RESULTS

Results of Microanalysis

Forty cassiterites from various localities were analyzed with the electron microprobe. These were divided into three categories on the basis of the observed luminescence effects and kinds of impurities present in significate amounts. Table I shows the range of concentration observed for various impurities in the three types. Cassiterites of type I contain appreciable amounts of Ta and Nb in addition to Fe and Ti, are usually not zoned and exhibit no appreciable luminescence. They usually exhibit pleochroism in thin sections. Pleochroism in cassiterites has been associated with the presence of Ta and Nb by Liebenberg (1945) and others. Most type I cassiterites are from pegmatites, and they are often associated with (and mistaken for) columbite and tantalite.

Cassiterites of the second type contain appreciable Fe and Ti, usually no W, no Ta or Nb and exhibit fine parallel zoning with moderate to strong yellow luminescence. Cassiterites of type III differ from type II by containing moderate amounts of W, and exhibit moderate to strong blue luminescence zoning. Cassiterites of types II and III are of hydrothermal origin.

X-Ray Scanning Images for Type II Cassiterites

Figure 2a is a Ti x-ray scanning image of micron-scale zones for a different region but the same sample as shown in plate I(a) and (b). The concentration profile has a maximum of 0.75 wt. % near the center of the scan and a minimum of 0.20 wt. % on the right. Figure 2b shows the Fe scanning image for the same region. Fe concentration varies from none to a maximum of 0.37 wt. % in the bright zone to the left of

TABLE I

Average Composition and Range of Impurity Concentrations (Element Wt. %) in Cassiterites of Three Different Types

	Type I		Type II		Type III	
Element	Average	Range	Average	Range	Average	Range
Al	0.11	0.0 -0.66	0.12	0.0 -0.60	0.09	0.0-0.88
Si	0.05	0.0 -0.12	0.07	0.0 0.30	0.05	0.0-0.65
S	<0.005	0.0 -0.006	<0.005	0.0 -0.006	<0.005	0.0-0.03
Ti	0.08	0.0 -0.23	0.21	<0.005-0.79	0.13	0.0-1.14
Mn	0.04	0.01-0.24	<0.005	0.0 -0.01	<0.005	0.0-0.02
Fe	0.63	0.02-2.59	0.66	0.02 -2.26	0.18	0.0-1.65
Ta	1.97	0.07-4.48	-	-	-	-
Nb	0.58	0.02-3.31	-	-	-	-
W	<0.005	0.0 -0.14	<0.005	0.0 -0.22	0.21	0.0-0.84
Bal. Sn + O	96.5 wt. %		99.0 wt. %		99.3 wt. %	

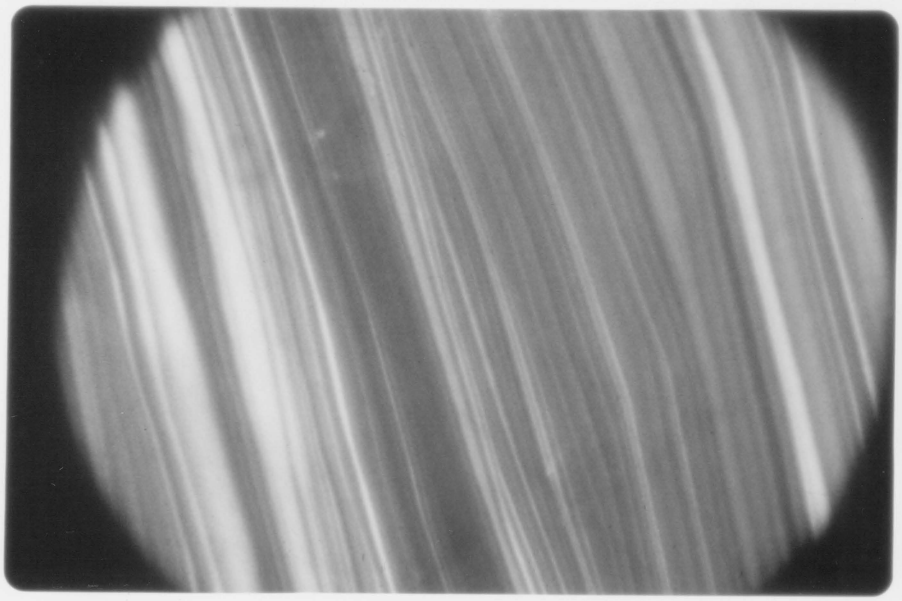

Plate I(a). Cathodoluminescence image of fine parallel zoning due to Ti-Fe impurities in a cassiterite of type II.

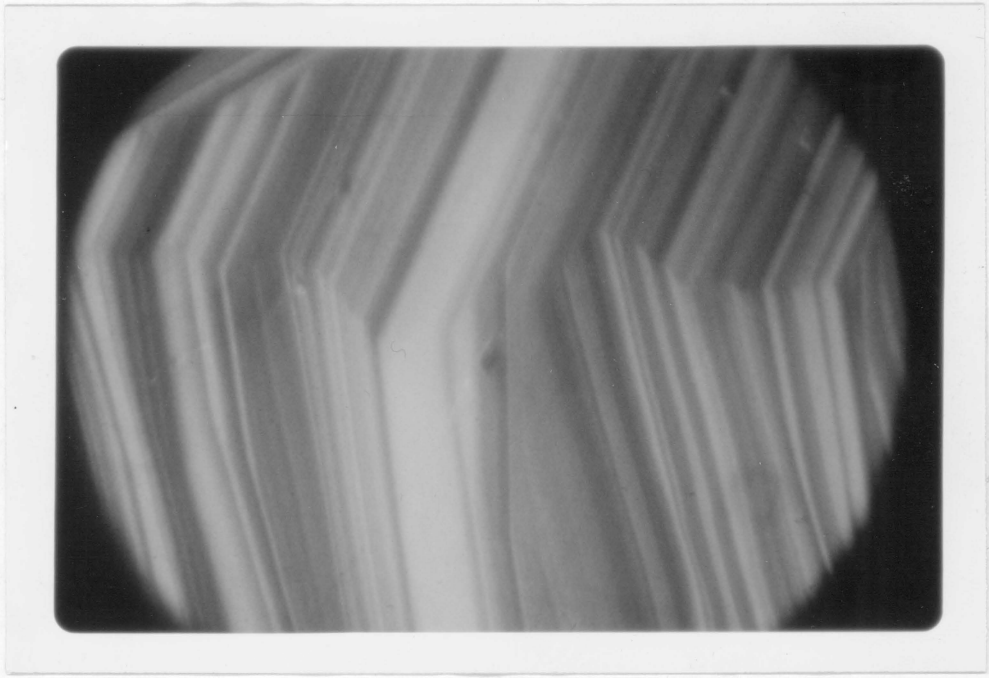

Plate I(b). Cathodoluminescence image for a type II cassiterite showing an irregular grain boundary. The true color is attenuated by absorption in a contaminating film which builds up on the sample surface during long exposures to electron excitation.

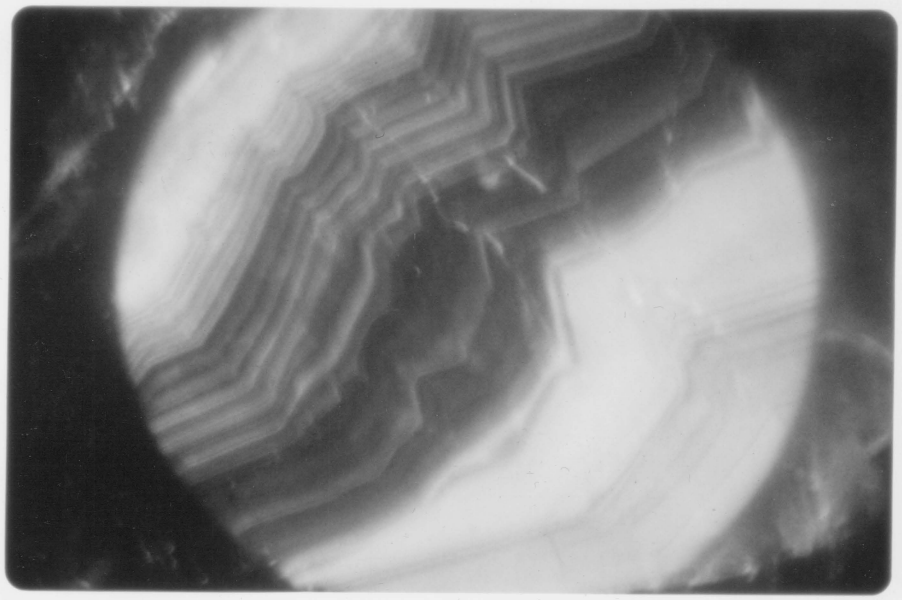

Plate I(c). Another sample of type II, this one showing extremely fine, irregular growth lamellae. Iron is segregated in different regions than Ti, the reddish-brown regions contain up to 1 wt. % Fe but almost no Ti while the bright zones on the upper right and lower left are Ti-rich.

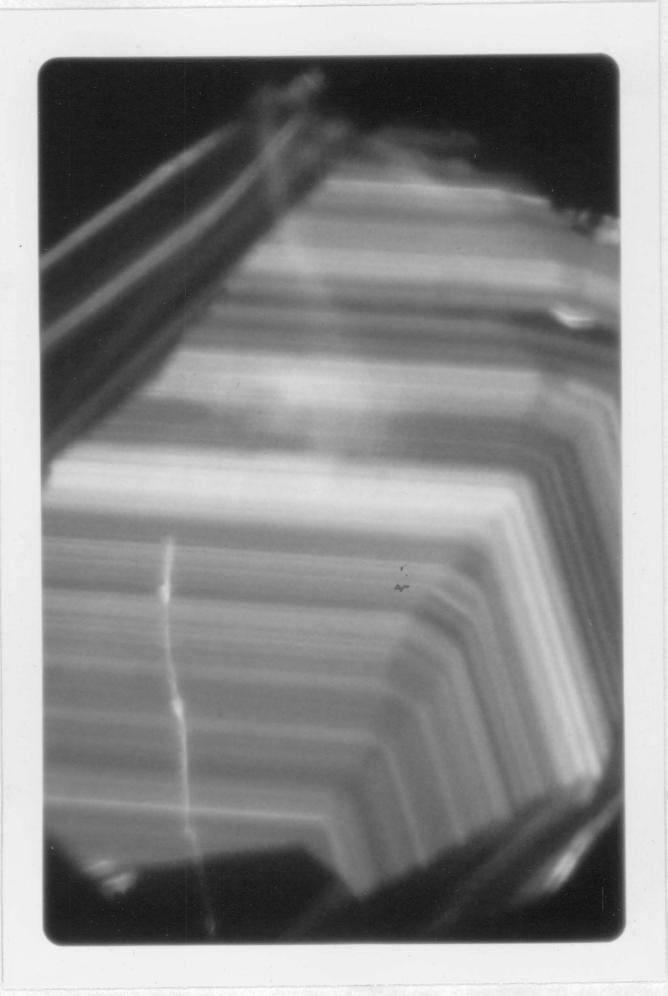

Plate I(d). Luminescence zoning for a W-bearing cassiterite. The apparent 3-D effect is due to regular crystal faces which are oblique to the polished surface.

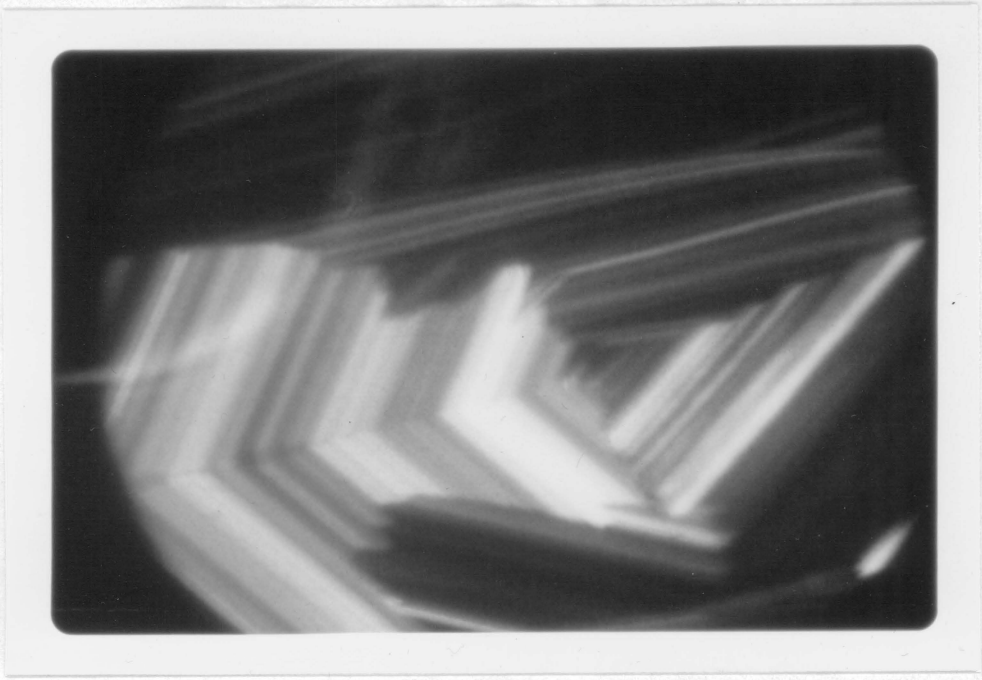

Plate I(e). A W-bearing, type III, cassiterite, showing an orange region which contains Ti and Si but is low in Fe and W. The dark regions contain large amounts of Fe.

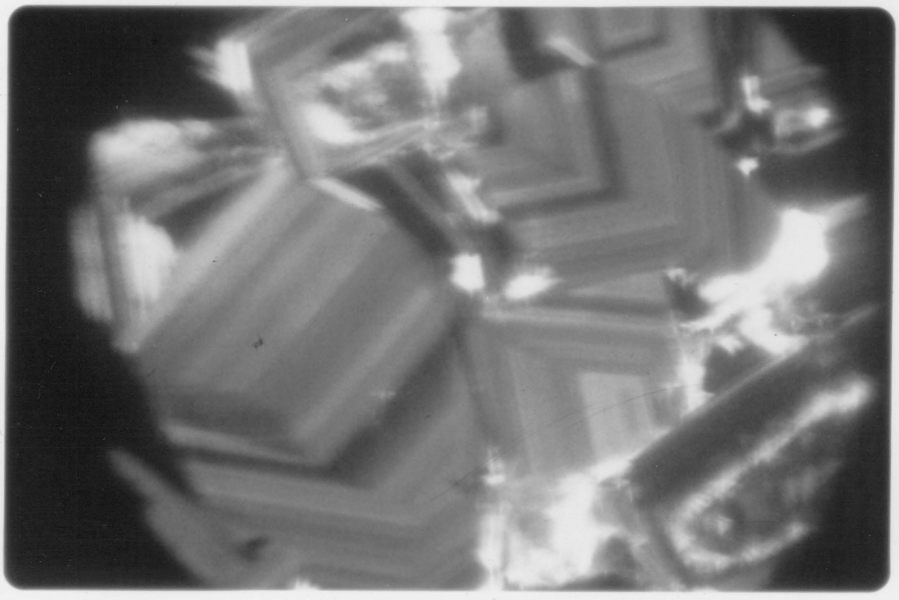

Plate I(f). A cluster of small crystals of W-bearing, type III cassiterite.

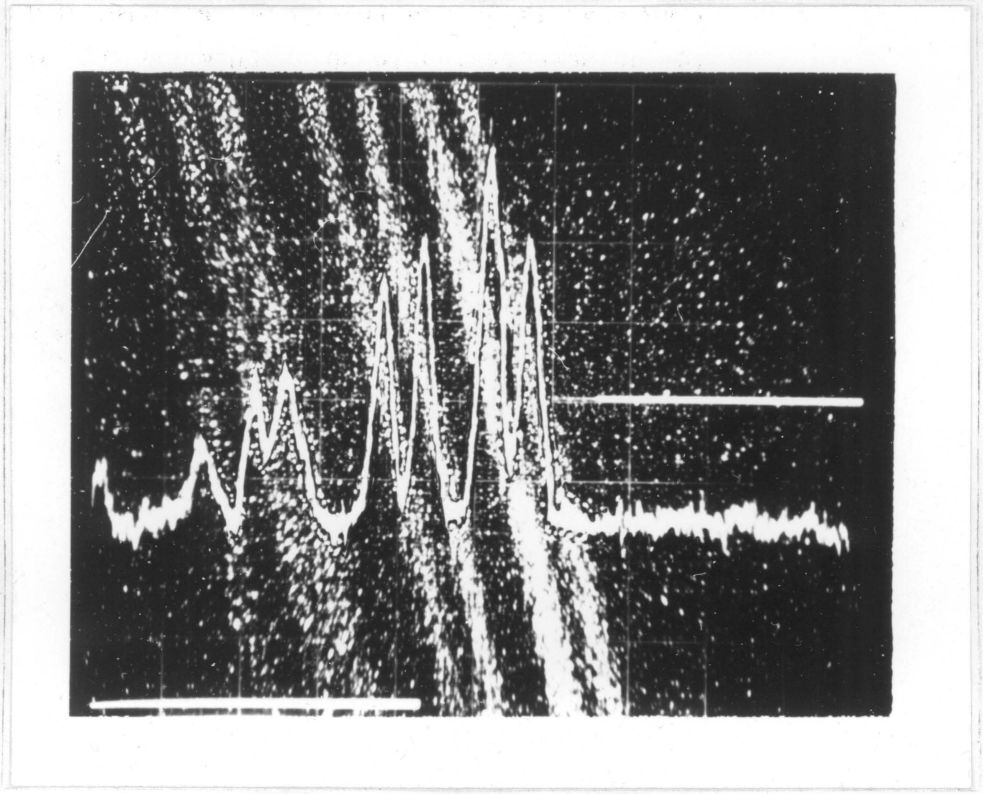

Figure 2a. Titanium x-ray scanning image for a zoned cassiterite which exhibits bright yellow-green cathodoluminescence in the zones of Ti and Fe concentration maxima. The scan region is 80 x 100 microns.

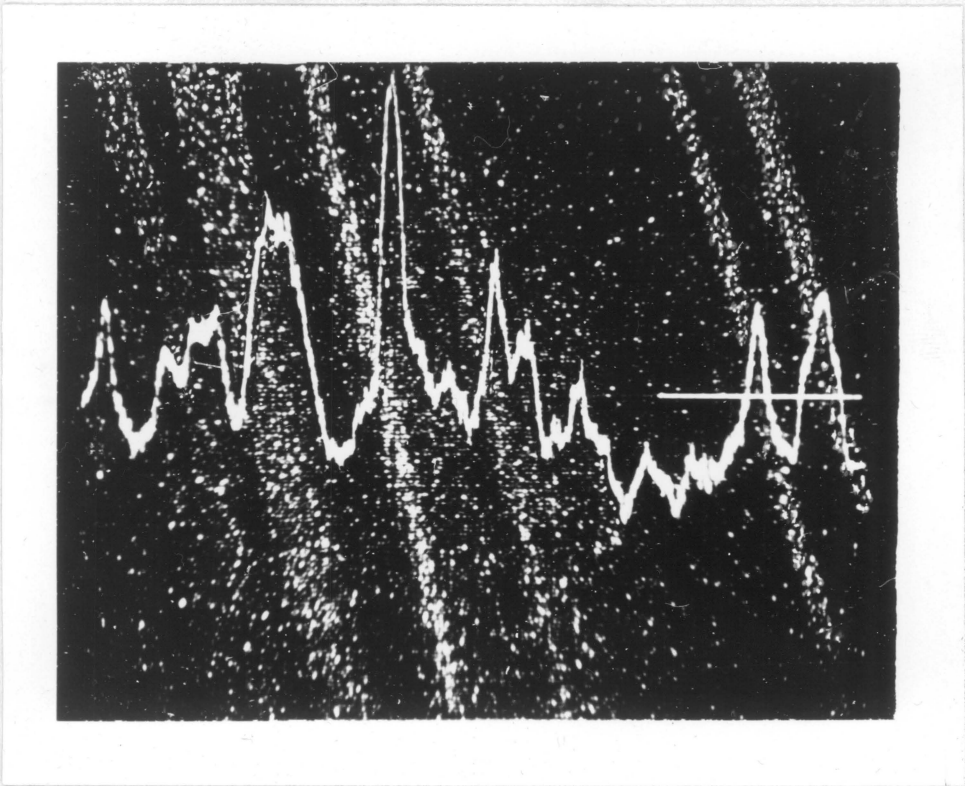

Figure 2b. Iron x-ray scanning image for the same region as Fig. 2a.

center. There are two zones of approximately 0.15 wt. % Fe appearing in the region at the right of this scan which exhibits no Ti zoning on the same scale, although generally Ti and Fe maxima tend to occur in the same regions. Bright yellow luminescence maxima are observed to occur where either or both Fe and Ti have maxima, indicating that Fe enhances the Ti-activated luminescence.

Luminescence and X-Ray Line Scanning Profiles

The line scanning profiles of Fig. 4 show the variation of luminescence with Ti and Fe concentration for a silicon free region of the same cassiterite as Fig. 3. The luminescence scan has been taken separately for the yellow (570 mμ) component and the blue (450 mμ) component. The intensity of the blue component is about half that of the yellow. The luminescence maxima tend to occur with maxima in the Fe concentration, with Ti maxima occurring in nearly the same regions. The Ti zoning is on an even finer scale than the observed luminescence zoning. This is due to the relatively poor resolution associated with the larger size of the luminescence excited region.

Figure 5 shows a series of profiles taken on a tungsten-bearing sample, a different region than that shown in Plate I(d). Note that Ti maxima generally correspond to strong luminescence peaks. Strong peaks in the blue luminescence scan occur where the W and Fe concentrations

Figure 3. Luminescence and x-ray line scanning profiles for a cassiterite exhibiting cathodoluminescence like that of Plate I(a) and (b).

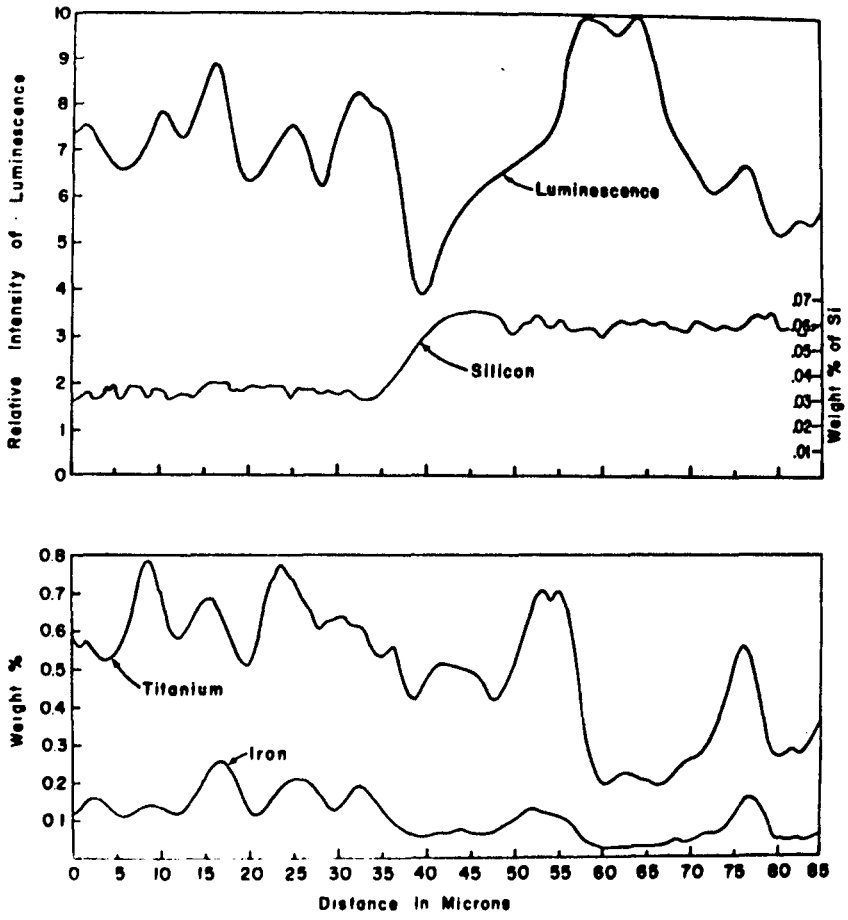
Relative Intensity of Luminescence
Luminescence
Silicon
Weight % of Si
Weight %
Titanium
Iron
Distance in Microns

Figure 4. Luminescence and x-ray line scanning profile for a different region of the same cassiterite as Fig. 3. The yellow and blue components were measured separately by using a linear interference filter which was set to pass yellow ($\lambda \sim 570$ mμ) and blue ($\lambda \sim 480$ mμ) radiation on consecutive scans of the same line.

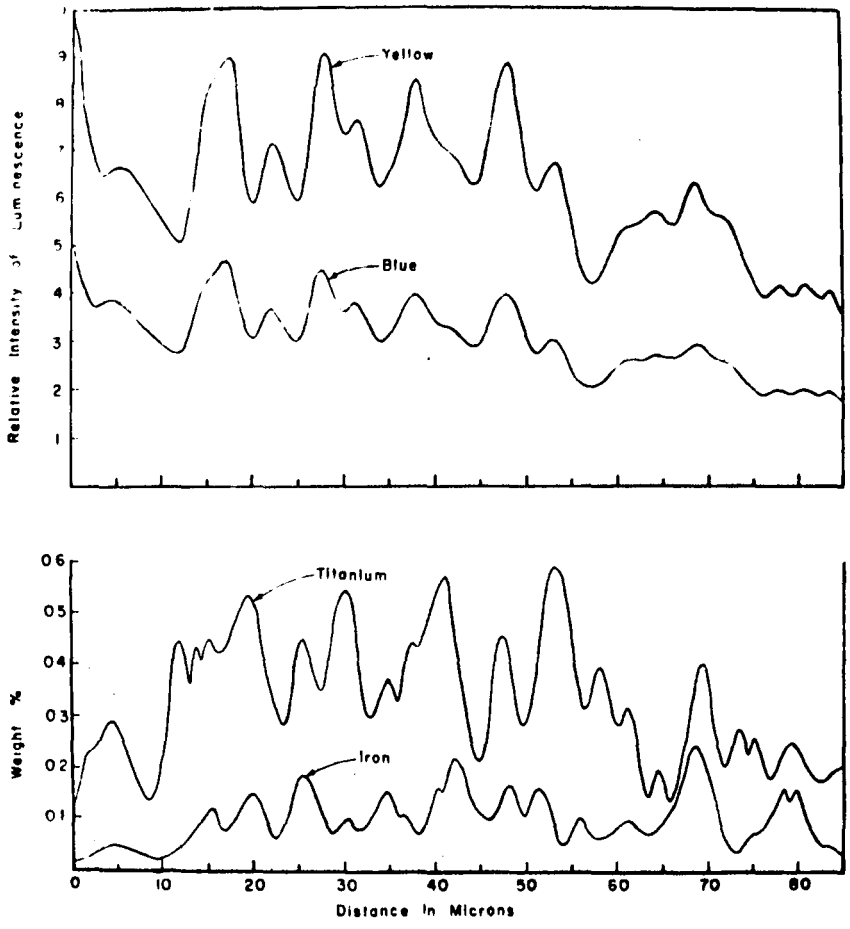
Yellow
Blue
Relative Intensity of Luminescence
Titanium
Iron
Weight %
0.6
0.5
0.4
0.3
0.2
0.1
0
10
20
30
40
50
60
70
80
Distance In Microns

Figure 5. Luminescence and x-ray line scanning profiles for a W-bearing cassiterite like that shown in Plate I(a).

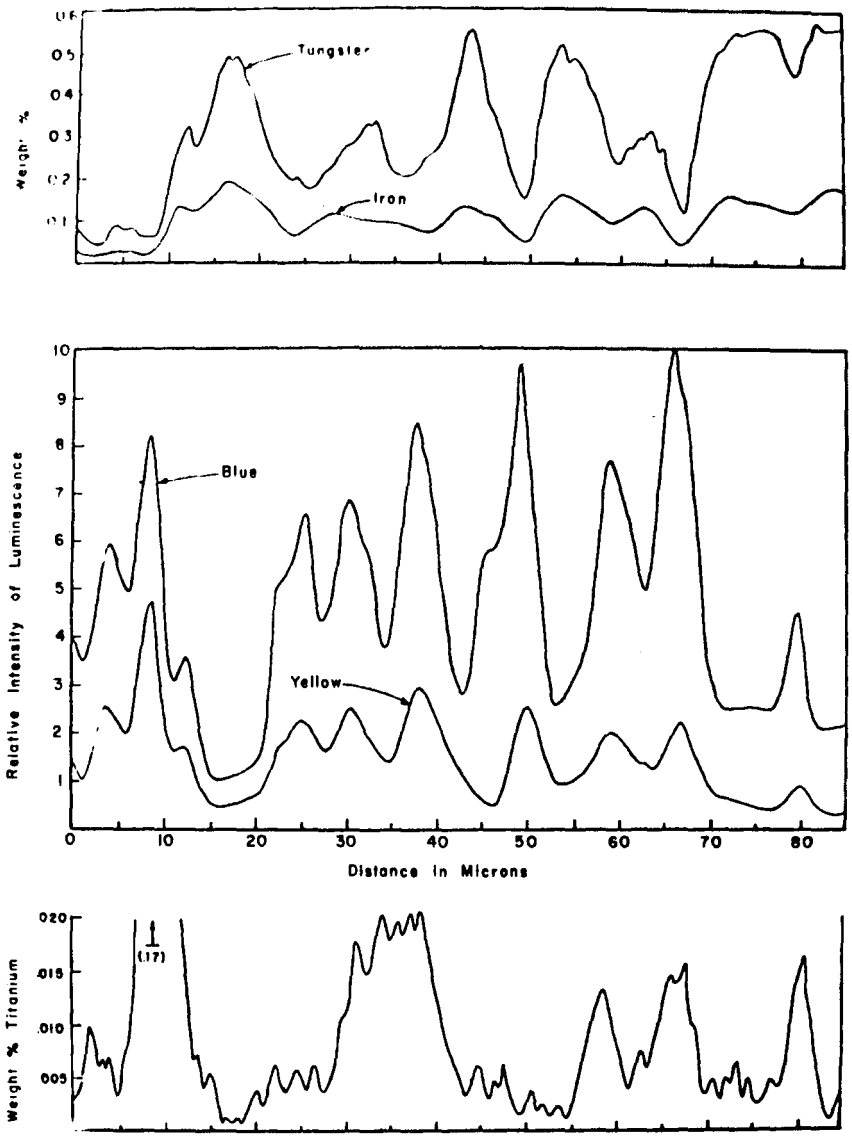
Tungsten
Iron
Blue
Yellow
Relative Intensity of Luminescence
Distance in Microns
Weight % Titanium
(17)

are low. The blue luminescent zones are not observed unless W is present, while the yellow zones are not observed unless Ti is present. Thus, W must change the role of Fe to make a quenching combination, while W in the absence of appreciable Fe gives luminescence with a strong blue component. Note that the concentration of Ti activators is generally less by a factor of 10 or more than for the Ti-Fe zoned sample. Visual observations indicate that Ti concentrations of less than 100 ppm. can activate strong luminescence when quenching combinations such as Fe-W, Fe-Si or Ta-Nb are absent.

X-Ray Scanning Images for Type III Cassiterites

The Ti, W and Fe x-ray scanning images and profiles on Figs. 6a, b and c were taken on a thin section of a specimen from the Dolcoath Mines, Camborne, Cornwall, England (M13865 of Table IV, Appendix B). Ti concentration ranges from less than 0.01% at the left to 0.23 wt. % in the bright bands left of center. Maximum W concentration is 0.27 wt. %, the partial scan at the center of the photograph indicates the background level of the W x-ray signal. The Fe concentration varies from less than 0.005 wt. % to 0.12% in the diffuse zone at the center. The partial scan, left of center, is background level, hence the weak resolution of Fe zoning in the scanning mode.

Emission Spectra

The cathodoluminescence spectra of Fig. 7 exhibits the typical bell-shaped form, which according to Vlam (1954) can be represented as

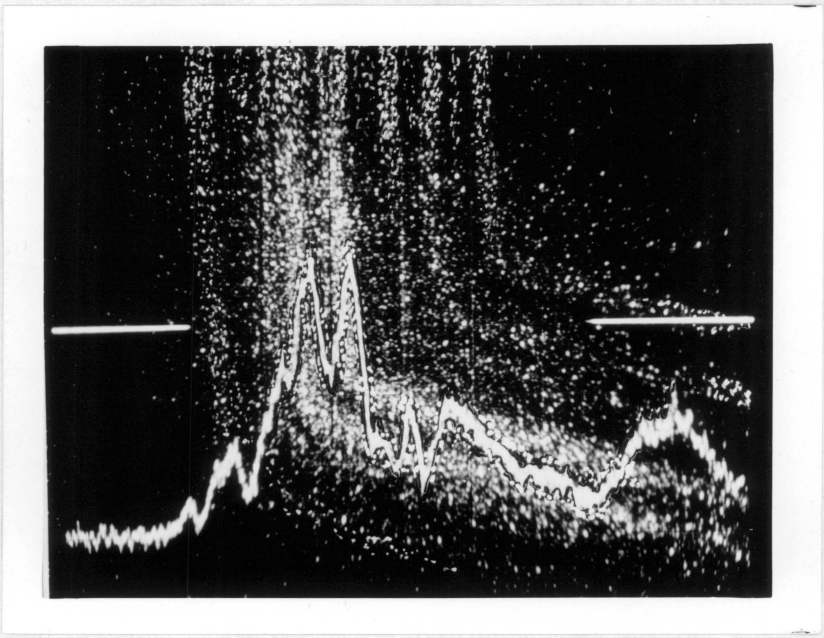

Figure 6a. Titanium x-ray scanning image for a cassiterite showing luminescence like that of Plate I(d). The scanned region is 80 x 100 microns. The line scan is across the center as indicated by the partial traces at the right and left of the photograph.

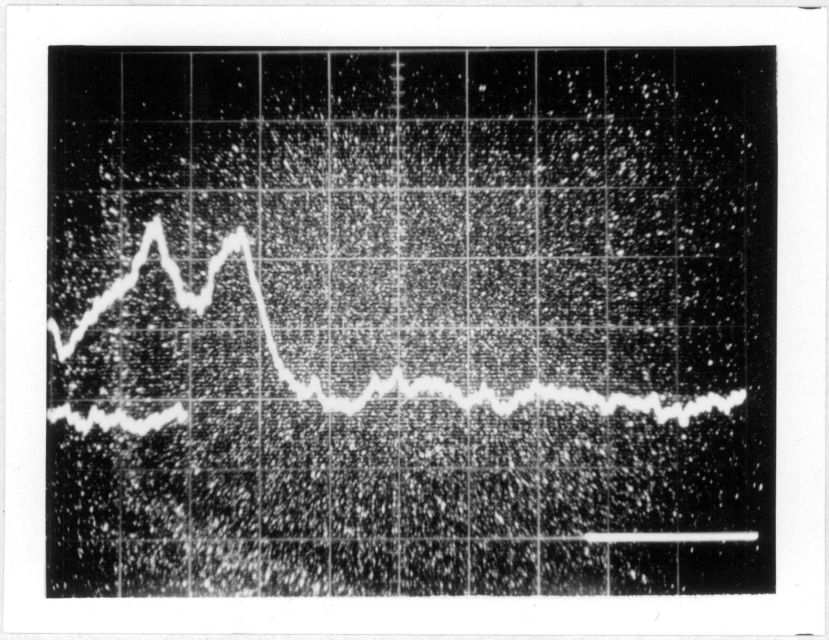

Figure 6b. Tungsten x-ray scanning image for the same region as Fig. 6a.

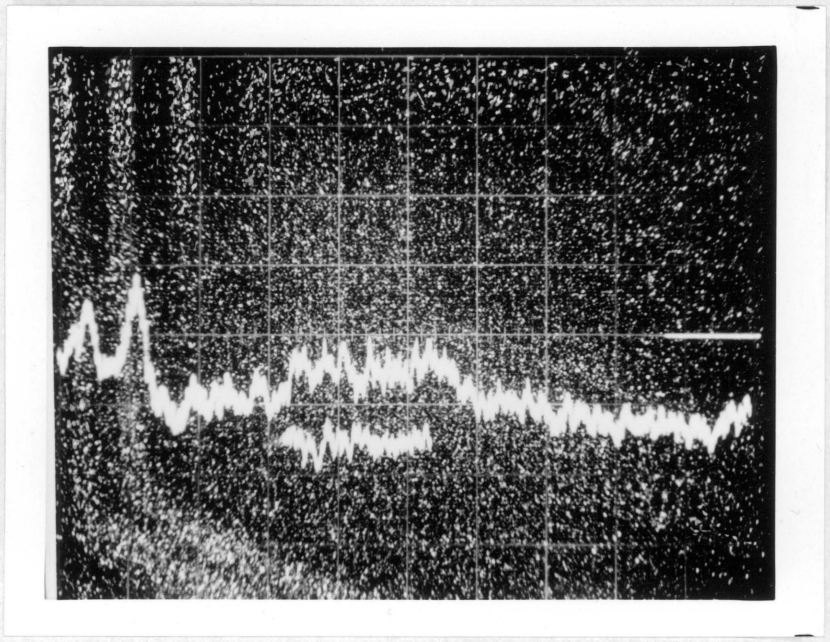

Figure 6c. Iron x-ray scanning image for the same region as Figs. 6a and 6b.

Figure 7. Typical spectral dispersion curves for Type II (Ti, Fe-activated) cassiterites and Type III (W, Ti-activated) cassiterites.

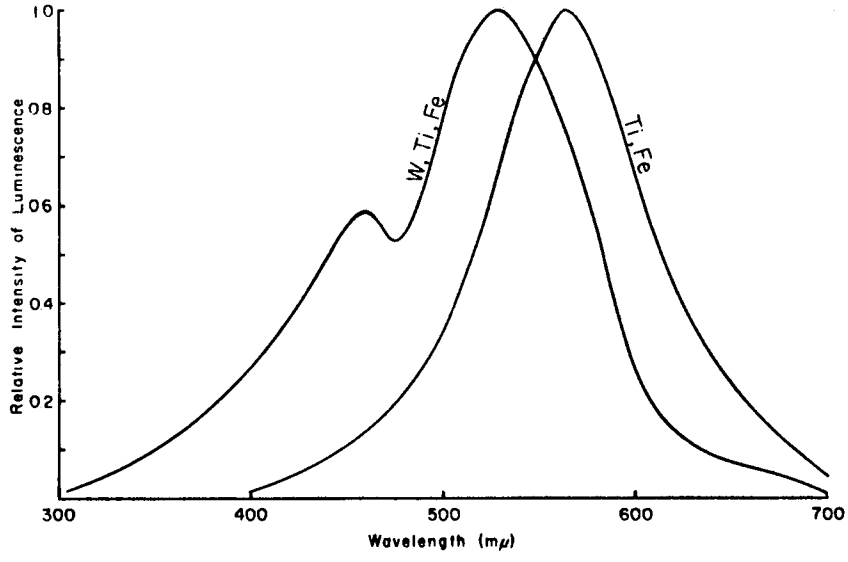
Relative Intensity of Luminescence
10
08
06
04
02
300
400
500
600
700
Wavelength (mμ)
W, Ti, Fe
Ti, Fe

a sum of Gaussian distribution functions when energy (intensity/wavelength) is plotted versus wavenumber. These indicate an emission band centered at about 565 mμ for Ti, Fe activated cassiterite, and two distinct emission bands for W, Ti activated cassiterite. The emission band centered near 440 mμ is evidently due to the presence of W and is essentially the same as that observed by Leverenz (1946) for self-activated calcium tungstate. The emission band due to the Ti ion in the W-bearing cassiterite appears to be shifted (~ 20 mμ) to shorter wavelengths.

Duration of the Luminescence

The decay time for cathodoluminescence of a type II, Ti-activated cassiterite measured at ambient temperature (Fig. 8) is $1.68 \pm .05 \times 10^{-4}$ seconds. Garlick (1949) points out that cathodoluminescence decay is often much more rapid than that for the same emission due to ultraviolet excitation. The more rapid decay of cathodoluminescence is related to the greater density of excitation by an electron beam than for excitation by ultraviolet radiation. Electron excitation tends to saturate deep traps and to fill a larger proportion of shallow traps, which decay rapidly, as compared with ultraviolet excitation which tends to fill deep traps rather than shallow ones. A temperature-dependent phosphorescence associated with deep trapping states has been noted for some phosphors excited by cathode rays, notably Mn-activated willemite (Strange and Henderson, 1946).

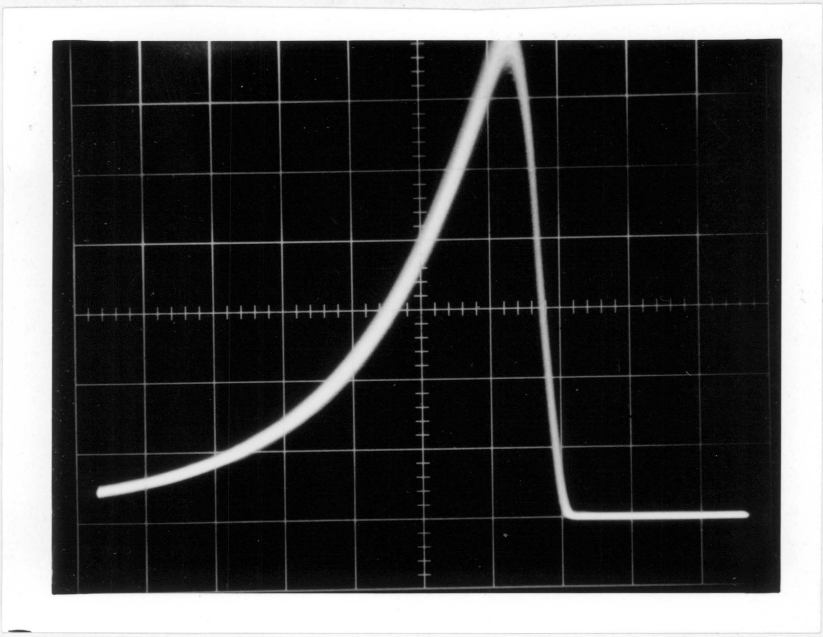

Figure 8. Rise-decay characteristics for cathodoluminescence of Ti-activated cassiterite. Right to left is the direction of increasing time. The rising curve affords a measure of the response time of the measuring system (~0.04 m sec.). The cathodoluminescence decay time (the difference between the fall-time and the rise-time) is $1.68 \pm .05 \times 10^{-4}$ seconds.

The decay time for cathodoluminescence of Ti-activated cassiterite is not temperature dependent in the range from 21°C to 275°C, so that trapping states do not appear to play an important role in the mechanism for luminescence.

Effect of Specimen Temperature on Cathodoluminescence

The intensity of the Ti-activated cathodoluminescence decreases rapidly with increasing specimen temperature (Fig. 9) and appears to be strongly quenched even at room temperature. Heated sample measurements were not made for W-activated cassiterite because of the difficulty of resolving the blue (440 mμ) band from the yellow-green (560 mμ) band. The Ti-activated emission spectrum at 473°K (Fig. 10) is shifted (~ 10 mμ) to shorter wavelengths as compared with that at 294°K, and is slightly broadened (~ 10 mμ) between the half-maximum intensity wavelengths. The intensity for each of the curves of Fig. 10 is relative to its own peak intensity and does not reflect the strong temperature quenching of Fig. 9, where intensity is relative to room temperature intensity.

Absorption Bands

A true absorption measurement requires the measurement of the intensity of the transmitted radiation lying within a narrow passband which is the same as the spectral profile of the illuminating source. Because of the Stoke's shift of the wavelength of the emitted radiation relative to that of the exciting radiation, this method minimizes the

Figure 9. Temperature dependence of the cathodoluminescence intensity ($\lambda \sim 565$ mμ) for a Ti-activated cassiterite.

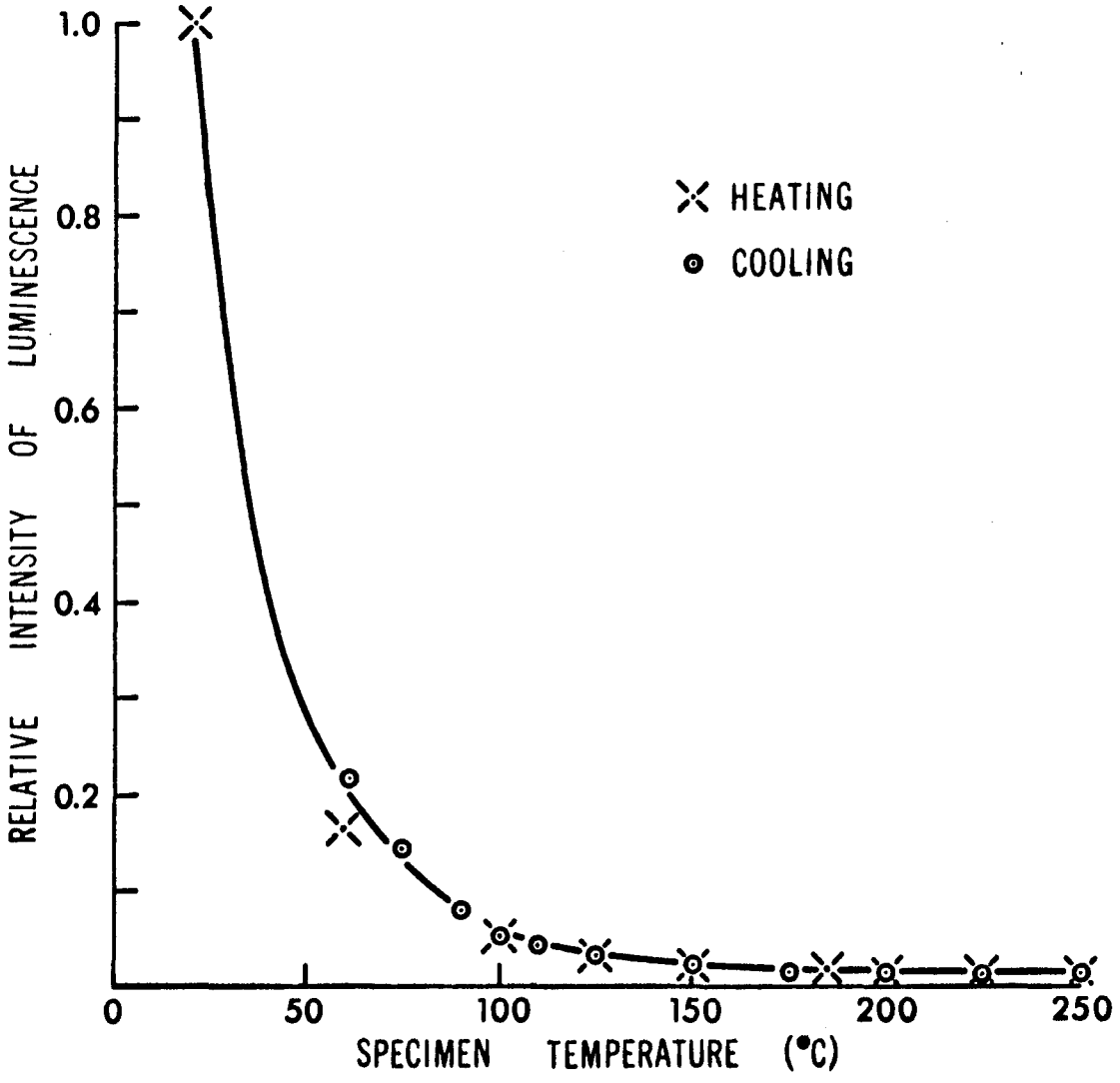
1.0
0.8
0.6
0.4
0.2
RELATIVE INTENSITY OF LUMINESCENCE
HEATING
COOLING
0
50
100
150
200
250
SPECIMEN TEMPERATURE (°C)

Figure 10. Cathodoluminescence spectra for a Ti-activated cassiterite at different temperatures.

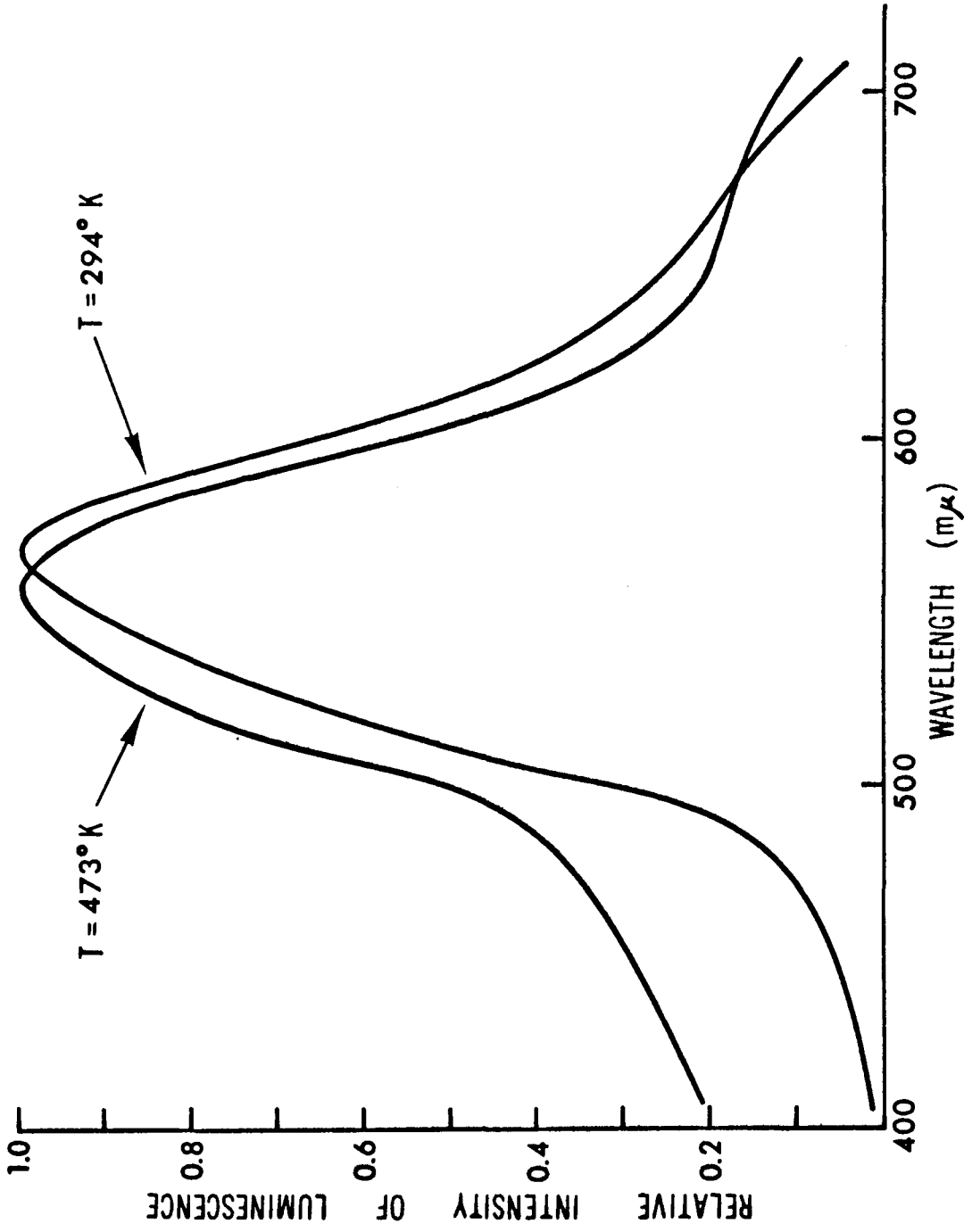
T = 294° K
T = 473° K
RELATIVE INTENSITY OF LUMINESCENCE
1.0
0.8
0.6
0.4
0.2
400
500
600
700
WAVELENGTH (mμ)

contribution to the observed transmission which is due to sample fluorescence. The absorption measurements made for this study do not yield true absorption data. A polychromatic source and one set of narrow bandpass filters were used in two different arrangements. In the first method the filters were placed between the source and the sample, giving a monochromatic source. If fluorescence is weak compared to the source intensity, this method yields results for sample absorption which are very nearly correct. In the second method the filters were placed between the sample and the detector. This method maximizes the effect of sample fluorescence and thus affords a determination of the fluorescence emission spectrum.

The results of these two types of measurements for a (Ti, Fe)-activated cassiterite and for a (W, Ti, Fe)-activated cassiterite are shown in Fig. 11. The absorption measurements for the two samples yielded essentially the same results, so that only one absorption curve is shown for both samples. The ultraviolet absorption is nearly complete over the entire range. This indicates that cassiterite is a small bandgap insulator ($E \sim 3.1$ ev.). There are two peaks in the absorption curve, one at 540 mμ ($E \sim 2.3$ ev.) and another at 645 mμ ($E \sim 1.9$ ev.).

The transmission measurements for the two samples are distinctly different and look very much like the typical emission spectra (see Fig. 7) superimposed upon a transmission curve which is the optical complement of the absorption curve. The transmission curve for the (Ti, Fe)-activated sample shows a peak at 565 mμ ($E \sim 2.2$ ev.) and another peak near

700 mμ may correspond to a weak red emission resulting from an Fe-activated transition which also corresponds to the second absorption peak (at 645 mμ).

The transmission curve for the (W, Ti, Fe)-activated sample shows a distinct emission peak at 440 mμ (E ~ 3.05 ev.) and a second peak near 540 mμ. The 440 mμ emission peak corresponds to the peak for W-activated cathodoluminescence, and would appear to be a transition between states near the extremes of the forbidden gap. The peak at 540 mμ may be attributed to Ti-activation and is shifted ~ 20 mμ toward shorter wavelengths with respect to the Ti emission peak for the (Ti, Fe)-activated sample. This shift corresponds exactly to that noted for the cathodoluminescence of the two types of sample (Fig. 7). Again, a weak red emission peak corresponding to an Fe-activated transition seems to be indicated at about 700 mμ.

Figure 11. Absorption curves for type I (Ti-activated) and type II (W, Ti-activated) cassiterites. The absorption curve was obtained with the interference filters between the source and the sample. The transmission curves were obtained with the interference filters between the sample and the detector.

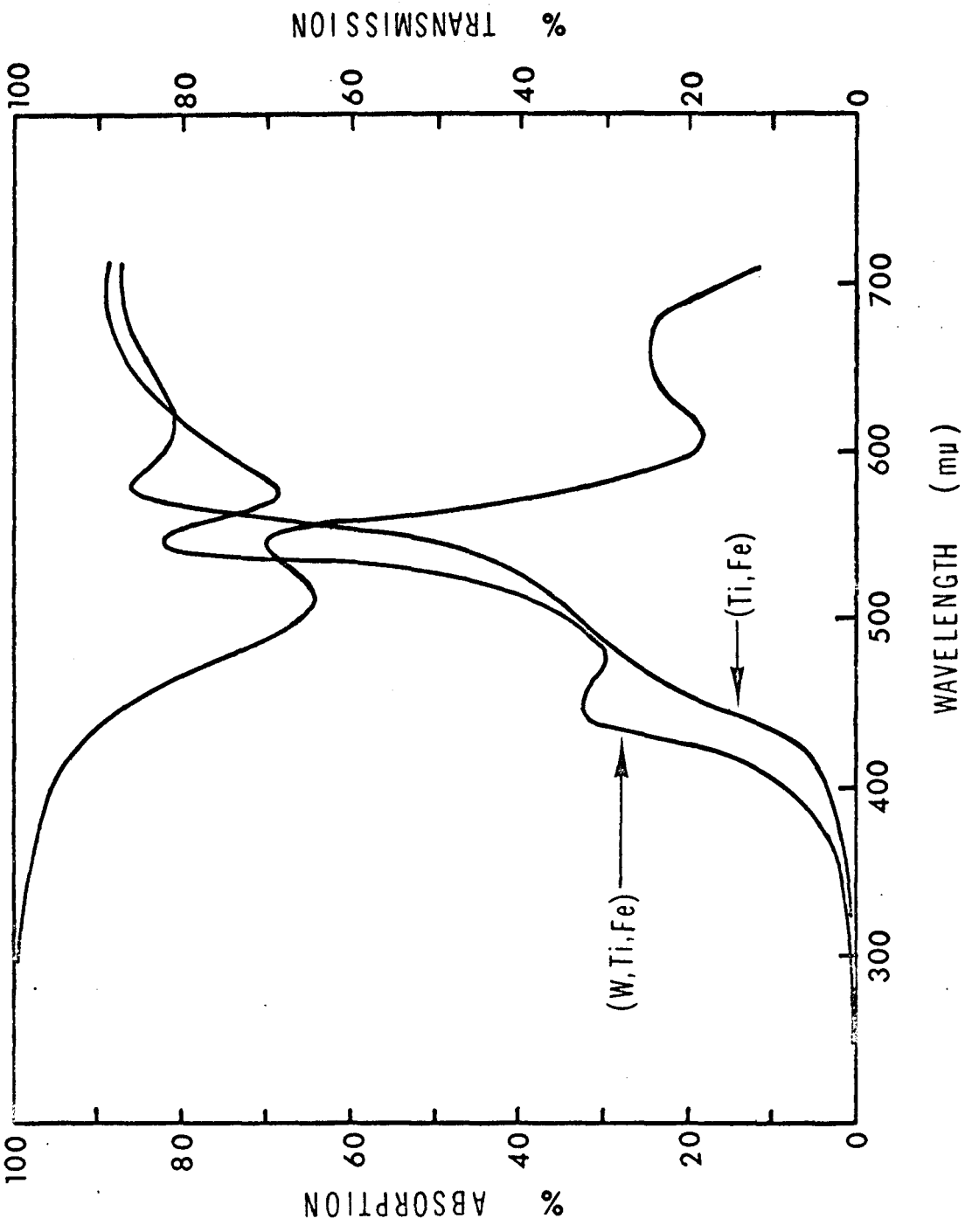
% TRANSMISSION
100
80
60
40
20
0
% ABSORPTION
100
80
60
40
20
0
300
400
500
600
700
WAVELENGTH (mμ)
(W,Ti,Fe)
(Ti,Fe)

V. DISCUSSION

The Ti-Activated Emission

The electron-excited broad yellow to yellow-green emission band of cassiterite is found to be associated with the presence of Ti, usually occurring with small amounts of Fe. The impurity combinations (Ta, Nb), (W, Fe) and (Si, Fe) act to quench the Ti-activated emission, while Fe in the absence of W and Si appears to enhance the cathodoluminescence. Since cassiterite has the rutile structure, substitution of Ti^{4+} for Sn^{4+} is expected. The structure of cassiterite was first determined by Vegard (1916) and later refined by Baur (1956) who gave the Sn-O distances as 2.052 Å and 2.056 Å and the comparable Ti-O distances as 1.944 Å and 1.988 Å. Kröger (1948) reports that Ti is almost universally effective for impurity-activated luminescence and has found both a long-wave excited yellow-green emission band, similar to the electron-excited emission for Ti-activated cassiterite, and a short-wave excited blue emission band for Ti-activated metastannates. Ti^{4+} in the perovskite structure of these metastannates is octahedrally coordinated with oxygen as it is in the cassiterite structure. Kröger concludes from measurements made on Ti-activated fluorides that the yellow-green emission is due to transitions in which the Ti^{4+} ion plays the dominant role, while the blue emission may be due to Ti and its associated oxygen atoms.

The Role of Fe

The Fe^{2+} and Fe^{3+} ions usually have a quenching effect on visible luminescence (Orgel, 1955) due to infrared transitions which are characteristic of these ions. However, a green emission band for magnesium aluminate spinel under cathode-ray excitation has been reported by Hummel and Sarver (1964) who attribute it to Fe^{3+} in tetrahedral coordination with oxygen. These workers also observed a deep-red band (near 700 mμ) which they suggest is probably due to Fe^{3+} in octahedral coordination with oxygen. The dark, reddish-brown, optically colored zones in cassiterite have been associated with the presence of Fe, primarily Fe^{2+} according to Mossbauer studies made by Grubb and Hannaford (1966) of color zoning in cassiterite. Both Fe^{3+} and Fe^{2+} are present in light and dark zones but Fe^{2+} is stronger in the dark zones which were also found to be ferromagnetic.

The concentration of Fe observed for cassiterite, as well as the ionic radii for the Fe^{3+} (~ 0.55 Å) and Fe^{2+} (~ 0.61 Å) ions as compared to that for the Sn^{4+} (~ 0.69 Å) ion, indicates that Fe substitutes for Sn and would, therefore, be in octahedral coordination with oxygen. This would seem to negate the possibility that Fe when not associated with W or Si produces a luminescence center distinct from that due to Ti. It seems more likely that the role of Fe in the luminescence process is strongly influenced by departures from stoichiometry. Since the available instrumentation for x-ray emission microanalysis is

not sufficiently sensitive for light element analysis to detect variations in the oxygen concentration of the order of 1% or less, a deficiency of oxygen in the luminescent versus the nonluminescent zones containing Fe and other impurities would have to be determined by other means. Such information, if obtainable, may shed some light on the conflicting behavior of Fe in the presence of W, Si, Nb and/or Ta as compared to its behavior when these impurities are not present.

The W-Activated Emission

The characteristic strong blue fluorescence of scheelite, when excited by ultraviolet radiation ($\lambda < 290$ mμ), has long been used in testing ores for the presence of this mineral. Leverenz (1946) has also observed blue luminescent bands ($\lambda \sim 485$ mμ) in the self-activated monoclinic tungstates $MgWO_4$, $CdWO_4$ and $ZnWO_4$. Randall (1939) has ascribed the emission to the presence of the tungstate ion WO_4^{2-}. The blue emission in cassiterite has nearly the same peak wavelength and spectral dispersion as that reported by Leverenz (1946) for $CaWO_4$ cathodoluminescence. The oxygen coordination of W in $CaWO_4$ would be tetrahedral as compared with the octahedral coordination of W in cassiterite, so that the results of this work would indicate that the W-activated emission is not strongly affected by the ligand field.

As was noted previously, Kröger (1948) found a blue emission band for Ti-activated stannates. Also, Smith (1949) has reported that

well crystallized diopside activated with Ti gives a broad blue emission band ($\lambda \sim 410$ mμ) under cathode-ray excitation. For cassiterite, however, the blue emission was never observed except in the presence of W. If the oxygen ligancy of Ti is responsible for the blue emission, as suggested by Kröger (1948), then we would expect that conditions favoring the blue emission might occur in the absence of W. Lacking such evidence, we may interpret the blue emission band for cassiterite to be characteristic of W-activation.

Effect of Ta and Nb

The combination (Ta, Nb) apparently acts to quench any luminescence which might otherwise occur. These ions also appear to be responsible for pleochroism in cassiterite. It is possible that these ions act to compensate for charge defects introduced by impurities such as Fe or by anion vacancies, but the exact nature of the mechanism is obscured by the effects of other impurities in natural cassiterite and will probably not be fully understood until measurements are made on synthetic crystals containing controlled amounts of impurities.

Intensity of the Cathodoluminescence

The variation in intensity of cathodoluminescence for fixed excitation conditions is a complex one due to the numerous interactions between the various types of impurity ions present in natural cassiterites. In the absence of quenching impurities, and at constant temperature, the

efficiency of luminescence is expected to depend on activator concentration, c, as follows (after Williams, 1966)

$$\eta = c(1-c)/[c + \nu (1-c)] \qquad (1)$$

where η is the ratio of emitted quanta to the number of excitations per second in the steady state, ν is the ratio of capture cross sections leading to nonradiative and radiative de-excitation. The number z depends on the spacial extent of the activator system, and, to a first approximation, is equal to the number of nearest neighbor sites. When quenching impurities are present the luminescence efficiency is reduced by processes which are usually not well enough understood to be treated theoretically. Coactivating or sensitizing impurities, such as Fe with Ti, introduce additional complex terms into the relationship for luminescence efficiency. Therefore the luminescence intensity profiles taken simultaneously with impurity concentration profiles (Figs. 3, 4 and 5) can only be interpreted qualitatively as denoting which impurities are activating, sensitizing or quenching the luminescence. It is possible to conclude from the presence of the cathodoluminescence specific to Ti- or W-activation that these impurities are present as trace elements even when x-ray counting statistics do not support this conclusion. When a luminescence mechanism has been found to be insensitive to the impurities which are known to be present, it is possible to extrapolate from luminescence intensity measurements to compositions of activator impurities which are lower than the limit of detectability in x-ray emission microanalysis.

Temperature Dependence

Since the energy of electrons in the exciting beam is much greater than the energy of thermal electrons, specimen temperature, within the experimental range, will have little effect upon the production of secondary electrons or upon the ionization of luminescence centers. Hence, the decrease of luminescence with increasing sample temperature is directly related to the nature of the center and relatively independent of the excitation mechanism (ultraviolet radiation, x-rays or high-energy electrons). Johnson (1966) states that, "The decrease in luminescence efficiency of all phosphors at elevated temperatures results generally from competing nonradiative de-excitation through a thermally activated process."

At high temperatures electrons from the full band (valence band) may be excited into empty ground states of the luminescence center or thermal disturbances may activate the return of electrons from the excited to the ground state of the center. If ξ is the activation energy for the thermal process, then the probability of this process is given by

$$p = \gamma \exp(-\xi/kT) \qquad (2)$$

where k is Boltzman's constant and T is the absolute temperature. The luminescence efficiency is then (Klasens, 1946)

$$\eta = L/L_o = 1/[1 + \gamma \sqrt{(\alpha J)} \exp(-\xi/kT)] \qquad (3)$$

where L_o is the luminescence intensity at low temperatures, J is a measure of the intensity of excitation and α is a constant for a particular luminophor and excitation process.

Since low temperature measurements were not made for this study, it is impossible to evaluate L_o and, therefore, not practical to try to fit the experimental data to a curve of the form of equation (3). However, since the factor $\gamma\sqrt{(\alpha J)}$ is typically of the order of 10^4 to 10^8, when $kT \gg \xi$, the exponential term is large compared to unity and equation (3) can be put into a form, valid for high temperatures, which does not involve L_o directly.

$$\ln L \simeq \ln L_o/\gamma\sqrt{\alpha J} + \xi/kT \qquad (4)$$

Thus for constant excitation, in the high temperature limit

$$\xi \simeq k \; d(\ln I)/d(1/T) \qquad (5)$$

When the cathodoluminescence intensity versus temperature data are evaluated with this equation, we obtain $\xi \simeq 0.015$ ev. Thus either the ground state of the luminescence center associated with Ti^{4+} is very close to the top of the valence band or the center is strongly perturbed by small thermal energy changes. It is worth noting that Kröger (1948) also found strong thermal quenching of the Ti-activated, ultraviolet excited luminescence of Ca, Sr and Ba metastannates.

If the luminescence center is closely coupled to the crystal or ligand fields, then as the temperature is increased the emission bandwidth will also increase due to the effect of greater thermal motion of ions surrounding the center. The emission spectrum for temperatures where no quenching occurs, is approximately a Gaussian distribution (Vlam, 1954) given by

$$L(\nu) = PQ_T \exp[-y^2 Q_T^2] \qquad (6)$$

where $y = (\nu - \nu_o)/\nu_o$, ν_o being the mean, or central, frequency of the emission band, P is a constant, $Q_T^2 = \tanh h\nu_e/2kT$, and $h\nu_e$ is the vibrational quantum energy of the excited state. The width at half peak intensity is

$$H(T) = H(0)\,[\coth(h\nu_e/2kT)]^{1/2} \qquad (7)$$

where $H(0) = 1.665/\sqrt{B}$, and $B = 2\pi hc^2\sqrt{\mu k_e}/k_g^2 r_o^2$. Where k_e and k_g are force constants in the ground and excited states respectively, μ is the effective vibrating mass, and r_o is the configuration coordinate for the minimum of the potential energy curve for the excited state of the center.

The observed emission bands for the Ti-activated luminescence (Fig. 9) are approximately Gaussian except for assymmetric side bands which are relatively more pronounced for the 473°K emission. These side bands may be the result of weak emissions produced by other defects or impurities in the crystal. The small (< 10 mμ) temperature

broadening of the 473°K spectrum compared to the room temperature spectrum indicates, according to equation (7), a high value for the vibrational quantum energy in the excited and ground states of the center.

A rule, which usually holds for metallic oxide phosphors as well as some sulfides and halides, formulated by Fonda (1957) relates the shift of spectral emission bands to changes in the anion-cation spacing of the compound. The basic reasoning is that the field strength to which the activator-center is subjected by its environment of oxygen atoms depends upon the anion-cation bondlengths. Substitution of a larger cation causes structural expansion and a reduction of the fields to which the luminescence center is subjected. As a result, the energy gap between the excited and ground states of the center increases and the luminescence emission band shifts to shorter wavelengths. The rule also holds for structural expansion and contraction due to temperature changes.

The shift ($\sim$ 10 mμ) of the emission band for Ti-activated cassiterite to shorter wavelengths is in accord with the rule cited above; however, the magnitude of the shift indicates that the Ti-center is not strongly disturbed by thermal motion of the oxygen ligands. The high value for the vibrational quantum energy of the excited state, as indicated by the small temperature broadening of the emission bandwidth, also supports this conclusion, which is in accord with Kröger's (1948)

conclusion that the Ti^{4+} ion plays the major role in determining the optical transitions which give rise to the yellow or yellow-green emission bands. The strong temperature dependence of the cathodoluminescence efficiency and negative evidence of thermally active electron traps, as well as the evidence of slight temperature broadening of the bandwidth and small band peak shift, all support the Klasens (1946) model for thermal quenching of the luminescence center. This model attributes thermal quenching to the filling of empty ground states of the luminescence center with electrons thermally excited from the valence band. The activation energy for this model is a measure of the energy difference between the ground state of the center and the top of the valence band, and is indicated to be small ($\sim$ 0.015 ev.).

It is worth noting that the orange luminescence (Plate I(e)) in the presence of Si^{4+} ($r \sim 0.40$ Å) substituting for Sn^{4+} ($r \sim 0.69$ Å) represents a shift of the Ti-activated yellow emission band in accord with Fonda's rule. On the other hand, the shift ($\sim$ 20 mμ) of the Ti-activated band in the presence of W^{4+} ($r \sim 0.65$ Å) is not in accord with this rule. The ionic radii are quoted from a recent study of effective ionic radii by Shannon and Prewitt (1968).

Absorption Spectra

The absorption and transmission curves of Fig. 11 indicate that the width of the forbidden band gap for cassiterite is of the order of 3.1 ev. The blue emission spectrum which is strong when tungsten is an impurity in cassiterite corresponds closely to a band to band transition.

Since the ionic radii of W^{4+} and Sn^{4+} are nearly the same, only small local disturbance of the SnO_2 energy band structure is to be expected.

All three elements (Ti, Fe, W) are transition metals. Ti and Fe with partially filled 3d and 4s levels and W with partially filled 5d and 6s levels would be expected to form normally empty bands in the forbidden region. The 2p level of the oxygen anion would provide a ground state for these defect band transitions. All three elements appear to produce excited states for luminescence transitions which are in accord with Fonda's rule and the quoted values of ionic radii.

SUMMARY

General

The intensity of cathodoluminescence in zoned cassiterites of hydrothermal origin has been determined, with the electron microprobe, to be directly related to the concentration of the luminescence activators Ti and W, provided no quenching combination (Fe, W) or (Ta, Nb) are present. Two distinct emission bands were observed, a yellow-green ($\lambda \sim 565$ mμ) band for Ti-activation and a blue ($\lambda \sim 440$ mμ) band for W-activation. The Ti-activated emission appears to be due to a luminescence center of the same type as that responsible for the long-wavelength excited fluorescence of the metastannates of Ca, Sr and Ba (Kröger, 1948). The intensity of cathodoluminescence exhibits strong thermal quenching. The activation energy for the thermal de-excitation process is less than 0.015 ev. The temperature broadening and shift of the peak intensity for the Ti-activated emission are small ($\sim$ 10 mμ/200°C), indicating a high value for the vibrational quantum energy of the ground and excited states of the center. Fe appears to enhance the Ti-activated emission, either as a non-essential coactivator or by reducing thermal quenching at room temperature. The decay time for the Ti-activated cathodoluminescence was determined to be $1.68 \times 10^{-4} \pm .05$ sec. and exhibits no appreciable temperature dependence from 21°C to 275°C. Thus the luminescence transition associated with the Ti-activated emission appears to be a long fluorescence process. The W-activated emission appears to be due to a luminescence center of the

same type as that observed for self-activated $CaWO_4$ (Leverenz, 1946), although W in cassiterite occupies octahedral sites while W in scheelite occupies tetrahedral sites. The presence of Fe with W suppresses the tungsten-activated emission. Thus, Fe occurring with W is a luminescence "killer" while Fe occurring with Ti enhances the probability of luminescence transitions. In addition to producing a distinct blue luminescence band, W occurring with Ti, in the absence of appreciable Fe, causes a small ($\sim$ 20 mμ) short-wavelength shift of the peak intensity for the Ti-activated emission.

Cassiterites, usually from pegmatites, which contain Ta and Nb (up to 2.0 wt. %) in addition to Fe and Ti, are seldom zoned and exhibit no appreciable cathodoluminescence. Specimens containing Ta and Nb usually are pleochroic. It seems likely that both pleochroism and luminescence quenching are related effects due to the presence of Ta and Nb in cassiterites. The work of Bahezre *et al.* (1961) indicates that Ta and Nb occur in dark to reddish-brown zones together with Ti and Fe, while Grubb and Hannaford (1966) report that the Fe^{2+} ion is relatively more concentrated in ferromagnetic, optically dark zones of cassiterite. Thus, the high optical absorption in cassiterites containing the ferrous ion in addition to Ta and Nb suppresses visible cathodoluminescence.

An orange cathodoluminescence emission was observed when Si is present with Ti in the absence of Fe, while Si occurring with Fe quenches visible cathodoluminescence.

Suggestions for Further Research

It appears that much valuable research utilizing the cathodoluminescence effect in conjunction with x-ray emission microanalysis could be performed if the electron microprobe were provided with a cold stage. The magnitude of thermal and impurity or defect quenching of luminescence is reduced at low temperatures so that it may be feasible to make measurements for luminescence bands which are too weak to be detected at room temperature. A more linear relationship should usually be observed for low activator concentrations in phosphors at low temperatures even in the presence of some types of quenching impurities or crystal defects. A more accurate diagnosis of impurity activators and quantitative determinations of concentration levels in the ppm range would thus be facilitated. The information to be gained from measurements of the temperature dependence of the luminescence intensity, spectral distribution and decay time and from measurements of the optical absorption bands for samples in thin section can lead to the choice of an appropriate model for the luminescence center and to a knowledge of the electronic and vibrational energy levels involved in luminescence transitions. Thermoluminescence measurements such as

those reported by Medlin (1963) for minerals could also be made during microanalysis.

The use of a dispersive device with better resolving power than is possible with the narrow band-pass filters used for this study would make it possible to observe fine structure in some luminescence spectra. Certain phosphors activated by rare earth elements (Eu, Gd, Sm, Tb, Dy) exhibit narrow-line luminescence due to transitions of internal 4f electrons which are shielded from the effects of crystal and ligand fields.

More accurate measurements of cathodoluminescence intensity rise-time and fall-time would also be facilitated if the electron microprobe were modified to provide a pulsed excitation and equipped with a photo-detector system having a response time in the range of 10^{-9} seconds or better. These modifications and additional equipment would involve a cost which is very small compared to the original cost of the electron microprobe.

As with most new areas of research in the early stages, cathodoluminescence studies of natural minerals and synthetics will have to be largely confined to the detailed cataloging of numerous effects until a sufficient mass of observations have been collected to permit a fairly complete classification. The application of solid-state theory and the use of the technology of solid-state research will provide the

mineralogist with a better understanding of geological materials. The information gained from such solid-state oriented studies of natural materials can, in turn, lead to improvements in solid-state theory and technology.

APPENDIX A

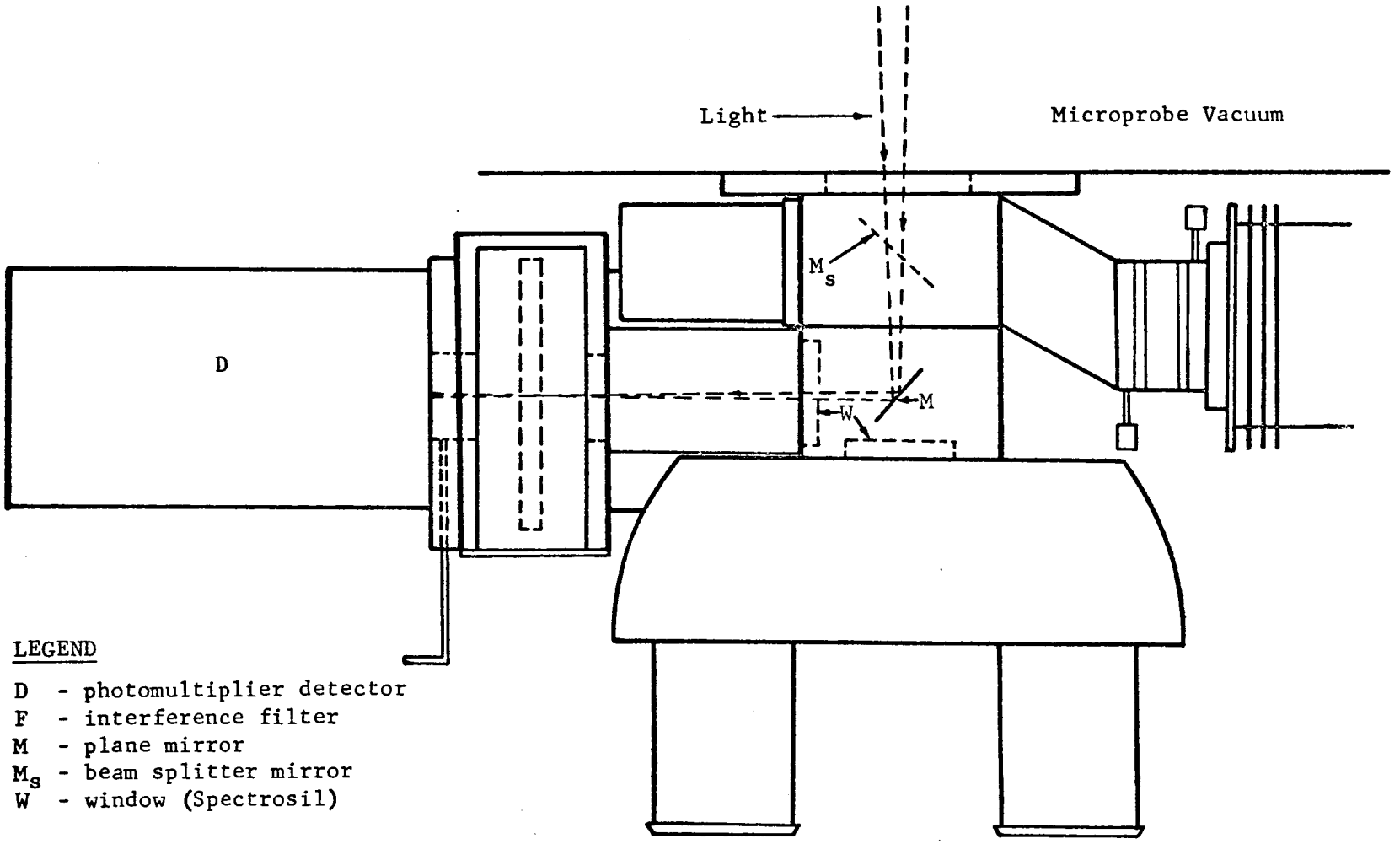

Figure 12. Sketch of microprobe modifications for luminescence measurements.

APPENDIX B

Corrections to the X-Ray Data

The x-ray data were corrected for deadtime, background and drift and averaged for each sample. Corrections for absorption, fluorescence and the atomic number effect were carried out on an IBM 360 computer system using the following programmed formulae:

Philibert's (1965) absorption correction

$$F(\chi) = \frac{1 + h}{(1 + \chi/\sigma)\,[1 + h(1 + \chi/\sigma)]}$$

where $\chi = (\mu/\rho)_m \csc \phi$, $\phi = 52.5°$ take off angle, $(\mu/\rho)_m$ sample mass absorption coefficient, $\sigma = 4.5 \times 10^{-5}/(E_o^{1.65} - E_c^{1.65})$ where $E_o = 20KV$ and E_c is the critical excitation potential, and $h = 1.2\,\bar{A}/\bar{Z}^2$.

A combination of Castaing's (1951) and Wittry's (1962) fluorescence correction for elements with $Z \leq 35$

$$G = \frac{\omega_k^B}{2} \cdot C_B \cdot \left(\frac{r-1}{r}\right) \cdot \frac{A}{B} \cdot \frac{\mu_B^A}{\mu_B^X} \cdot \left[\frac{U_B \ln U_B - U_B + 1}{U_A \ln U_A - U_A + 1}\right] \cdot \left[\frac{\ln(1+u)}{u} + \frac{\ln(1+v)}{v}\right]$$

where ω_k^B is the k-fluorescence yield, C_B is the concentration of element B, r is the absorption jump ratio, A and B are the atomic weights of elements A and B, μ_B^A (μ_B^X) are the mass absorption coefficients of element A (the sample) for the characteristic radiation of element B. $U_A = E_o/E_c^A$, $U_B = E_o/E_c^B$, $u = \chi_A/\mu_B^X$, and $v = \sigma/\mu_B^X$.

The atomic number correction of Thomas (1963)

$$K = C_i\alpha_i / \sum_{j=1}^{n} C_j\alpha_j$$

with $\alpha_i = S_i/R_i$ where S_i, the stopping power of the i'th element, is from Nelms (1956, 1958) data, and the R_i are those given by Thomas.

TABLE II

Average Composition and Range of Impurity Concentrations (Element Wt. %)
for Type I Cassiterites

Specimen	Al	Si	S	Ti	Mn	Fe	Nb	Ta	W
M8657 Black Hills, South Dakota	0.068 0.03-0.16	<0.005 0.0-0.08	0.014 0.01-0.02	0.084 0.07-0.12	0.056 0.03-0.07	0.77 0.20-1.25	0.85 0.57-1.47	3.02 1.19-4.48	<0.005 0.0 -0.01
M8658 Black Hills, South Dakota	0.104 0.07-0.15	<0.005 0.0-0.06	0.012 0.01-0.02	0.162 0.15-0.17	0.024 0.02-0.03	0.433 0.33-0.78	0.015 0.0 -0.05	2.30 1.96-2.84	<0.005 0.0 -0.03
M8659 Custer, South Dakota	0.118 0.0 -0.61	0.043 0.0-0.21	0.019 0.0 -0.12	0.059 0.04-0.07	0.026 0.0 -0.09	0.580 0.31-0.86	0.651 0.12-1.04	1.56 0.73-2.70	- -
M16180 Silver Hills, Washington	0.089 0.03-0.16	0.133 0.0-0.68	<0.005 0.0 -0.008	0.070 0.05-0.1	0.084 0.0 -0.24	0.710 0.26-1.38	1.11 0.38-3.31	1.66 0.50-3.73	- -
M18655 Unknown Locality	0.040 0.0 -0.11	<0.005 0.0-0.01	- -	0.035 0.0 -0.05	0.020 0.0 -0.05	0.63 0.33-0.85	0.85 0.58-1.02	1.65 1.37-1.94	- -
M5542 Unknown Locality	0.070 0.02-0.11	0.041 0.0-0.69	<0.005 0.0 -0.009	0.146 0.04-0.23	0.009 0.0 -0.012	0.066 0.03-0.13	0.199 0.07-0.54	0.135 0.07-0.26	0.096 0.07-0.14
UC1713 Hill City, South Dakota	0.072 0.03-0.18	<0.005 0.0-0.02	- -	0.058 0.04-0.07	0.011 0.0 -0.02	0.241 0.14-0.46	0.381 0.29-0.46	0.81 0.59-1.07	- -
UC3606 Bear Gulch, South Dakota	0.297 0.06-0.66	0.024 0.0-0.05	0.010 0.0 -0.02	0.046 0.02-0.07	0.024 0.0 -0.1	1.59 1.03-2.59	0.565 0.16-1.37	4.65 2.56-7.69	0.055 0.0 -0.32

TABLE III

Average Composition and Range of Impurity Concentrations (Element Wt. %) for Type II Cassiterites

Specimen	Al	Si	S	Ti	Mn	Fe	Nb,Ta	W
MA56417 Malaysia	0.062 0.0 -0.10	<0.005 0.0-0.02	0.008 0.0 -0.02	0.212 0.02-0.54	<0.005 0.0 -0.01	0.427 0.02-0.70	- -	- -
M4992 Sts. of Malacca	0.084 0.04-0.11	<0.005 0.0-0.06	0.011 0.0-0.02	<0.005 0.0 -0.02	0.014 0.0 -0.02	0.021 0.02-0.03	-	-
UC___ Swaziland	0.033 0.02-0.05	0.183 0.0-0.56	<0.005 0.0 -0.01	0.348 0.30-0.42	<0.005 0.0 -0.01	0.014 0.01-0.02	-	-
M1661 Ringaroonia District	1.11 0.0 -2.60	0.774 0.0-2.18	<0.005 0.0 -0.008	0.543 0.45-0.65	<0.005 0.0 -0.008	0.364 0.06-0.97	-	<0.005 0.0-0.19
M13862 Durango, New Mexico	0.208 0.12-0.34	0.018 0.0-0.08	- -	0.006 0.0 -0.012	<0.005 0.0 -0.02	1.42 0.70-2.62	-	<0.005 0.0-0.16
M13868 Durango, New Mexico	0.052 0.0 -0.19	0.051 0.0-0.09	0.013 0.01-0.02	<0.005 0.0 -0.008	0.137 0.12-0.15	0.724 0.25-1.16	- -	- -
M13863 Mexico	0.044 0.03-0.06	- -	0.008 0.0 -0.01	0.611 0.32-1.02	0.010 0.0 -0.02	0.058 0.02-0.11	-	0.026 0.0-0.22
M5542 Quanajuato, Mexico	0.009 0.0 -0.02	- -	- -	<0.005 0.0 -0.02	- -	1.65 1.45-1.81	- -	- -

TABLE III (Continued)

Specimen	Al	Si	S	Ti	Mn	Fe	Nb,Ta	W
UC2151 Schlagenwald, Bohemia	0.031 0.02-0.09	0.027 0.0-0.07	<0.005 0.0-0.01	0.331 0.04-0.55	- -	0.026 0.01-0.05	- -	- -
UC293 Schienfriedersdorf, Saxony	0.034 0.02-0.08	- -	0.007 0.01-0.02	0.298 0.15-0.53	- -	0.076 0.02-0.18	- -	<0.005 0.0-0.10
M1481 Ehrenfriedersdorf, Saxony	0.117 0.06-0.17	- -	0.009 0.01-0.02	0.523 0.33-0.88	0.015 0.01-0.02	0.065 0.03-0.122	- -	<0.005 0.0-0.03
M13859 Winslow, Maine	0.124 0.0-0.34	- -	- -	0.193 0.12-0.33	- -	0.136 0.07-0.28	- -	- -
M11277 Unknown Locality	0.033 0.01-0.11	0.061 0.0-0.11	0.007 0.0-0.01	0.003 0.0-0.008	0.014 0.0-0.02	3.88 2.42-4.96	- -	- -
M1484 Cornwall, England	0.210 0.06-0.54	- -	0.014 0.02-0.04	0.017 0.0-0.03	0.010 0.0-0.02	0.602 0.01-1.21	- -	<0.005 0.0-0.08
UC1 Unknown Locality	0.008 0.0-0.02	0.012 0.0-0.03	- -	0.257 0.18-0.36	- -	0.122 0.02-0.18	- -	0.024 0.0-0.12
UC2 Unknown Locality	0.016 0.0-0.05	<0.005 0.0-0.04	- -	0.264 0.1-0.79	<0.005 0.0-0.01	0.462 0.03-0.62	- -	0.064 0.0-0.15

TABLE III (Continued)

Specimen	Al	Si	S	Ti	Mn	Fe	Nb,Ta	W
UC4	0.010	0.08	-	0.204	-	0.082	-	0.042
Unknown Locality	0.0-0.02	0.0-0.02	-	0.02-0.36	-	0.03-0.11	-	0.0-0.12
UC8	0.013	0.011	-	0.224	<0.005	0.224	-	-
Unknown Locality	0.0-0.02	0.0-0.02	-	0.0-0.33	0.0-0.01	0.01-0.36	-	-

TABLE IV

Average Composition and Range of Impurity Concentrations (Element Wt. %) for Type III Cassiterites

Specimen	Al	Si	S	Ti	Mn	Fe	Nb,Ta	W
M13865 Cornwall, England	0.094	0.065	0.009	0.109	0.011	0.154	-	0.145
	0.03-0.20	0.01-0.15	0.0-0.02	0.01-0.23	0.0-0.02	0.01-0.30	-	0.01-0.61
M13866 Cornwall, England	<0.005	-	-	0.277	-	0.064	-	0.338
	0.0-0.03	-	-	0.16-0.43	-	0.02-0.23	-	0.0-0.66
M9739 Germany	0.077	0.069	0.016	<0.005	0.012	0.583	-	0.399
	0.03-0.12	0.0-0.18	0.01-0.03	0.0-0.006	0.0-0.02	0.39-1.65	-	0.0-0.60
M13867 Germany	0.123	0.020	<0.005	0.121	<0.005	0.245	-	0.558
	0.05-0.26	0.0-0.20	0.0-0.006	0.04-0.22	0.0-0.009	0.09-0.38	-	0.10-0.84
UC295 Schlagenwald, Bohemia	0.098	0.034	<0.005	0.413	-	0.114	-	0.149
	0.04-0.35	0.0-0.06	0.0-0.008	0.09-1.14	-	0.07-0.22	-	0.03-0.42
M1498 Schagenwald, Bohemia	0.008	0.023	<0.005	0.218	-	0.087	-	0.138
	0.0-0.01	0.0-0.07	0.0-0.01	0.14-0.56	-	0.02-0.15	-	0.0-0.51
M16432 Bohemia	0.187	0.084	<0.005	0.025	-	0.088	-	0.125
	0.02-0.69	0.0-0.48	0.0-0.006	0.0-0.06	-	0.01-0.28	-	0.0-0.68
M16462 Bohemia	0.056	0.152	<0.005	0.151	0.008	0.133	-	0.037
	0.0-0.34	0.0-0.65	0.0-0.01	0.05-0.28	0.0-0.02	0.0-0.73	-	0.0-0.11

TABLE IV (Continued)

Specimen	Al	Si	S	Ti	Mn	Fe	Nb,Ta	W
UC292 Cornwall, England	0.031 0.02-0.05	0.024 0.0-0.05	<0.005 0.0-0.01	0.028 0.01-0.08	<0.005 0.0-0.01	0.060 0.03-0.10	- -	0.288 0.0-0.70
UC3605 Tasmania	0.055 0.04-0.08	- -	0.012 0.0-0.03	0.172 0.04-0.38	- -	0.056 0.03-0.10	- -	0.223 0.0-0.66
M1677 Sts. of Malacca	0.005 0.0-0.01	- -	0.018 0.01-0.02	0.160 0.10-0.27	- -	0.235 0.02-0.80	- -	0.148 0.0-0.37
M13218 Araca, Bolivia	0.011 0.02-0.06	0.014 0.0-0.06	<0.005 0.0-0.006	0.014 0.0-0.02	- -	0.030 0.01-0.05	- -	0.189 0.0-0.46
M13861 California	0.322 0.13-0.70	0.067 0.0-0.31	0.006 0.0-0.01	0.088 0.02-0.25	<0.005 0.0-0.01	0.612 0.33-0.99	- -	0.112 0.02-0.15
M16432 Unknown Locality	0.204 0.02-0.88	0.084 0.0-0.49	<0.005 0.0-0.006	0.024 0.0-0.06	- -	0.114 0.01-0.32	- -	0.128 0.0-0.68

BIBLIOGRAPHY

Bahezre, Par C., Capitant, M. et Duong, Phas Kien (1961). Analyse ponctuele d'une cassiterite zonée. Bull. Soc. Franc. Miner. Crist., LXXXIV, pp. 321-2.

Baur, W. H. (1956). Über die Verfeinerung der Kristallstrukturbestimmung einiger Vertreter des Rutiltype; TiO_2, SnO_2, GeO_2 und MgF_2. Acta Cryst., Vol. 9, pp. 515-20.

Bloch, F. (1928). Über die Quantenmechanik der Elektronen in Kristallgittern. Z. Phys., Vol. 52, p. 555.

Castaing, R. (1951). Applications des Sondes Électroniques à une Méthode d'Analyse Ponctuelle Chimique et Cristallographique. Ph.D. Thesis, University of Paris, 140 pp.

Fonda, G. R. (1957). Influence of activator environment on the spectral emission of phosphors. J. Opt. Soc. Am., Vol. 47, pp. 877-80.

Garlick, G. F. J. (1949). Luminescent Materials. Oxford Clarendon Press, London, p. 183.

Grubb, P. L. C. and Hannaford, P. (1966). Ferromagnetism and color zoning in some Malayan cassiterite. Nature, Vol. 209, p. 677.

Hall, M. R. and Ribbe, P. H. (1968). An electron microprobe study of luminescence centers in cassiterite (abstract). Geol. Soc. Am., Southeastern Sect. Ann. Meeting, Durham, N. C.

Heinrich, K. F. J. (1963). Instrumental developments for electron microprobe readout. Advan. X-Ray Anal., Vol. 7, pp. 291-300.

von Hippel, A. (1936). Einige prinzipielle Gesichtspunkte zur Spektroskopie der Ionenkristalle und ihre Anwendung auf die Akalihalogenide. Z. Phys., Vol. 101, pp. 680-720.

Hummel, F. A. and Sarver, J. F. (1964). The cathodoluminescence of Mn^{2+}- and Fe^{3+}-activated magnesium aluminate spinel. J. Electrochem. Soc., Vol. 111, pp. 252-3.

Kröger, F. A. (1948). Some aspects of the luminescence of solids. Elsevier Publishing Company, New York, pp. 158-73.

Klasens, H. A. (1946). Centres in zinc sulphide phosphors. Nature, Vol. 158, p. 306.

Kyser, D. F. and Wittrey, D. B. (1964). Cathodoluminescence in gallium arsenide. The Electron Microprobe, Proc. Electrochem. Soc., eds. McKinley, T. D., Heinrich, K. F. J. and Wittrey, D. B. John Wiley and Sons, New York, pp. 691-714.

Johnson, P. D. (1966). Oxygen-dominated lattices. Luminescence of Inorganic Solids, ed. Goldberg, P. G., Academic Press, New York, pp. 287-336.

Lambe, J. and Klick, C. C. (1955). Model for luminescence and photoconductivity in the sulfides. Phys. Rev., Vol. 98, p. 909.

Leverenz, H. W. (1946). Final report of research and development leading to new and improved radar indicators. R.C.A. report, PB25481. Office of the Publication Board, Dept. of Commerce, Wash., D. C.

Liebenborg, W. R. (1945). Notes on the occurance of a pleochroic variety of cassiterite in South Africa. Trans. Geol. Soc. S. Africa, Vol. 48, p. 1.

Medlin, W. L. (1963a). Emission centers in thermo-luminescent calcite, dolomite, magnesite, aragonite, and anhydrite. J. Opt. Soc. Am., Vol. 53, pp. 1276-85.

_____ (1963b). Thermoluminescence in quartz. J. Chem. Physics, Vol. 38, pp. 1132-43.

_____ (1963c). Thermoluminescence of sedimentary rock. 6th World Petroleum Congress. Frankfort, Main, Germany.

Nelms, A. T. (1956). Energy loss and range of electrons and positions. NBS Circ. No. 577.

_____ (1958). Suppl. to NBS Circ. No. 577.

Orgel, L. E. (1955). Phosphorescence of solids containing the manganous or ferric ions. J. Chem. Physics, Vol. 23, p. 1958.

Philibert, J. (1956). L'analyse quantitative en micro-analyse par sonde électronique. Publ. Inst. Rech. Siderurgie (Saint-Germain-en-Laye), Sér. B, No. 51.

Randall, J. T. (1939). Some recent experiments in luminescence. Trans. Faraday Soc., Vol. 35, p. 2.

Ribbe, P. H. and Hall, M. R. (1965). Microprobe cathodoluminescence and x-ray emission studies of cassiterite (abstract). Geol. Soc. Am. Ann. Meeting, Kansas City, Missouri.

Schön, M. (1942). Zum Leuchmechanismus der Kristallphosphors. Z. Physik, Vol. 119, p. 463.

Seitz, F. (1938). Interpretation of the Properties of KCl:Tl Phosphors. J. Chem. Phys., Vol. 6, p. 150.

_____ (1939). An Interpretation of Crystal Luminescence. Trans. Faraday Soc., Vol. 35, p. 74.

Shannon, R. D. and Prewitt, C. T. (1968). Effective ionic radii in oxides and fluorides. Acta Cryst. (in press).

Smith, A. L. (1949). Some new complex silicate phosphors containing calcium, magnesium, and beryllium. J. Electrochem. Soc., Vol. 96, pp. 287-96.

Smith, J. V. and Stenstrom, R. C. (1965). Electron-Excited Luminescence as a Petrologic Tool. J. Geol., Vol. 73, pp. 627-35.

Strange, J. W. and Henderson, S. T. (1946). Cathodoluminescence. Proc. Phys. Soc. (London), Vol. 58, p. 368.

Thomas, P. M. (1963). Outline of a method for correcting for atomic number effects in electron probe microanalysis. Brit. J. Appl. Physics, Vol. 14, pp. 397-98.

Vegard, L. (1916). Results of crystal analysis. Phil. Mag., Ser. 6, Vol. 32, p. 65.

Vlam, C. C. (1954). The shape of the emission bands of luminescent solids. Brit. J. Applied Physics, Vol. 5, pp. 443-46.

Williams, F. (1966). Theoretical basis for solid-state luminescence. Luminescence of Inorganic Solids, ed. Goldberg, P. G., Academic Press, New York, p. 36.

Wittrey, D. B. (1962). Fluorescence by characteristic radiation in electron-probe microanalysis. U.S.C.F.C. Rept., Univ. of Southern Calif., Los Angeles, pp. 84-204.

The vita has been removed from the scanned document

AN ELECTRON MICROPROBE STUDY OF LUMINESCENCE CENTERS IN CASSITERITE

by

Monte R. Hall

ABSTRACT

An electron microprobe equipped with a device for making luminescence measurements has been used to determine the concentration of luminescence activators in zoned cassiterites of hydrothermal origin. Micron-scale growth zones contain variable amounts of Ti, Fe, W and other impurities. The impurity ions replace Sn^{4+} to produce luminescence centers. The relative intensity of cathodoluminescence and the amount and kind of impurity activators were simultaneously measured while scanning the growth zones with a micro-focussed electron beam.

Two distinct emission bands were observed, a yellow-green ($\lambda \sim$ 565 mμ) band for Ti-activation and a blue ($\lambda \sim$ 440 mμ) band for W-activation. Measurements made on a heated sample show strong thermal quenching of the Ti-activated cathodoluminescence. The decay time for the Ti-activated emission, which is independent of temperature from 21°C to 275°C, is 0.168 msec. The cathodoluminescence spectrum for W-activation closely resembles that of self-activated $CaWO_4$ (Leverenz, 1946) although a higher oxygen coordination (VI) for W in cassiterite is to be expected. Fe occurring with Ti appears to enhance the Ti-activated emission. Fe occurring with W or Si quenches luminescence.